ISAS - INTERNATIONAL SCHOOL FOR ADVANCED STUDIES

Thesis submitted for the degree
of
"MAGISTER PHILOSOPHIAE "

" BAND STRUCTURE AND LANDAU LEVELS IN SEMICONDUCTOR SUPERLATTICES : BAND MIXING EFFECTS "

Candidate	Supervisor
Dr. Francesco Ancilotto	Dr. Annalisa Fasolino

Academic Year 1985/86

TRIESTE

SISSA - SCUOLA
INTERNAZIONALE
SUPERIORE
DI STUDI AVANZATI
TRIESTE
Strada Costiera 11

ACKNOWLEDGEMENTS

I want to express my gratitude to Annalisa Fasolino for her invaluable help and for her patient support during the preparation of the manuscript.

I am also indebted to Jan C. Maan for an enlightening discussion.

Finally, I want to thank Furio Ercolessi, who gave me several useful suggestions in the noble art of computer programming.

INTRODUCTION

This thesis is concerned with the effect of mixing of hole subbands in Quantum Wells on the optical transitions in a magnetic field.

The recent improvement in epitaxial growth techniques has made possible to realize high-quality semiconductor heterostructures: magneto-optical experiments on these systems have revealed in the observed spectra complex structures that cannot be accounted for by simple models of quantum confinement. More detailed band structure calculations seem necessary in order to explain the observed features : however, the strong non-linear behavior of the Landau levels and the relaxation of the usual selection rules for optical transitions resulting from the coupling between hole subbands, have precluded up to now a convincing comparison between theory and experiments.

We show that with the explicit evaluation of the transition strengths, in a six-band envelope- function approach, a detailed and almost complete agreement with the observations is achieved. The qualitative details of the calculation depend critically on the sample parameters, implying the possibility of their precise determination through the comparison between the theory and magneto-optical experiments.

The layout of the thesis is as follows :

Chapter I contains an introductory review on the electronic properties of Semiconductor Heterostructures ;

Chapter II describes the method, based on the Envelope-Function Approximation, that has been used in our energy level calculation;

in Chapter III illustrative examples of calculated subbands in Superlattices are reported: a brief account of two related topics is also given ;

Chapter IV deals with Excitons, in two and three dimensions ;

in Chapter V the calculated interband transition energies and strengths are compared with magneto-optical experiments on GaAs Quantum Wells;

Chapter VI is concerned with Cyclotron Resonance in Quantum Well's structures.

INDEX

CHAPTER I : GENERAL CONSIDERATIONS ABOUT SEMICONDUCTOR HETEROSTRUCTURES

CHAPTER II : THE ENVELOPE-FUNCTION APPROXIMATION

CHAPTER III : SUBBANDS IN QUANTUM WELLS AND SUPERLATTICES

CHAPTER IV : EXCITONS IN QUANTUM WELLS AND SUPERLATTICES

CHAPTER V : LANDAU LEVEL CALCULATION AND COMPARISON WITH MAGNETO-OPTICAL EXPERIMENTS

CHAPTER VI : CYCLOTRON RESONANCE IN TWO-DIMENSIONAL HOLE GAS

CHAPTER I

GENERAL CONSIDERATIONS ABOUT SEMICONDUCTOR HETEROSTRUCTURES

1. Introduction

The steady improvement in the thin-film growth techniques such as Molecular Beam Epitaxy (MBE) [1] or Metal Organic Chemical Vapor Deposition (MOCVD) [2] , has made possible to realize high quality semiconductor heterostructures composed of periodic sequences of ultrathin crystalline layers (10 ÷ 1000 Å) of alternating semiconducting compounds with interfaces sharp on an atomic scale : these artificial media exhibit novel properties not shown by their parent compounds in the bulk.
Interest in SuperLattices (SL), as these multilayer structures are usually called, originates from an early proposal [3] of a one-dimensional man-made "superlattice" having period shorter than the electron mean free path .
Table I gives a list of several SL systems, indicating where the major interest lies for each of them (from Ref.[5]).

These structures are generally grown alternating lattice-matched semiconductor compounds of group-III and group-V or group-II and group-IV elements; there are various reasons for this choice :

(1) these compounds have a direct band gap :this means that ,since they can emit or absorb light without the help of lattice vibrations, they are particularly suited for the realization of opto-electronic devices;

(2) they can be easily doped ;

(3) they can form various solid solutions with identical crystal structure and well-matched lattice parameters but with different energy band gaps.

An almost exhaustive list of closely-matched pairs of binary and elemental semiconductors ,including III-V/II-VI SL systems, is given in Ref.[6].

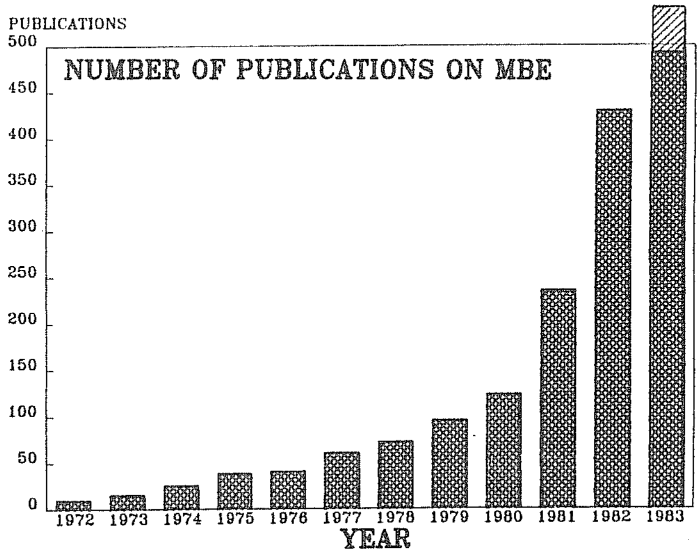

Fig.1

Fig. 1. Diagram of the number of technical papers on MBE of III-V compounds published in the period 1972 to 1983. The actual number in 1983 will increase by approximately 10 percent, because the collection of citations was finished by mid-December 1983

TABLE I. Semiconductor superlattices.

Systems	Techniques	Remarks
GaAs–GaAlAs(AlAs)	MBE, MOCVD, LPE	Extensively studied
InAs(InGaAs)–GaSb(GaSbAs)	MBE	Extensively studied
GaSb–AlSb	MBE	Metallurgical and optical properties
InAs–AlSb	MBE	Optical and magnetoproperties
GaAs(GaP)–GaAsP	MOCVD, CVD	Strained superlattice, luminescence
GaAs–InAs(InGaAs)	MBE, MOCVD	Metallurgical and light-emitting properties
InP–InGaAs	MOCVD	Magnetoproperties
InP–InGaAsP	LPE	Light-emitting properties
InSb–GaSb	Sputtering	Ordered structure, interdiffusion
GaP–AlP		Theoretical indirect-direct gap
Ge–GaAs(GaAlAs)	MBE	Metallurgical properties, defects
Si–SiGe	MBE, CVD	Dislocations, mobility enhancement
CdTe–HgTe	MBE	Zero-finite gap, metallurgical profiling
PbTe–PbSnTe	Hot-wall	Interdiffusion, magnetotransport
PbTe–PbGeTe	MBE	Dislocations, Auger profiling
InAs–GaSb–AlSb	MBE	Polytype superlattice and heterostructure
GaAs(n)–GaAs(p)	MBE	Doping superlattice, tunable gap

(from : L.L. Chang,
J. Vac. Sci. Technol. B 1 (2), Apr.–June 1983)

SL structures possess unusual electronic properties of quasi-two dimensional character. The simplest case is that of an undoped GaAs layer sandwiched between barrier-layers of $Al_xGa_{1-x}As$: the GaAs band gap is entirely contained within that of AlGaAs, the latter being a function of the alloy composition x (This is an example of the so-called "type-I" SL). The net potential is the sum of the potential in the A and B layer and of a square wave-shaped "superpotential" which arises from the band gap differences between A and B materials (fig.2). For the conduction band for example, the layers

Quantum-well structure and corresponding real-space energy band structure. The schematic diagram in a shows compositional profiling in thin layers. The circle in b represents an exciton in the bulk compound, and the ellipse represents an exciton confined in a layer with a low band gap. Figure 2

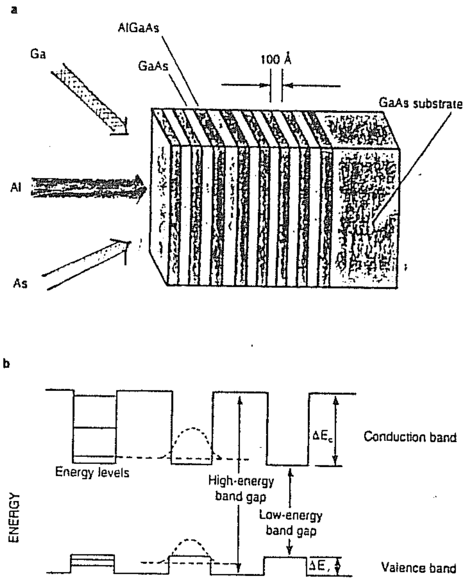

Fig.2

of one material -say A- form a series of square shape potential wells which confine the electrons in the conduction states. The quantized confinement energies are of the order of :

$$E_n = \pi^2\hbar^2 n^2 / 2m^* L_z \qquad , n=0,1,2.... \qquad (1.1)$$

where m^* is the effective band-edge mass for the electron and L_z is the width of the confining layer.
To each of these "particle-in-the-box" levels corresponds a two-dimensional density of states $m^*/\pi\hbar$ .For thick AlGaAs barriers, the associated wavefunctions are mainly localized in the A-layer, with evanescent wings in the adjacent B layers. In this case, the system is usually called a Quantum Well (QW).
However, if the decay length of the wavefunction in B-layer is comparable with the width of the barrier, tunnelling of electrons through these potential barriers can occur, leading to the formation of subbands having small but finite widths, which are the SL conduction bands.

Thus SL's present a duality of aspects, the QW aspect with quantized confinement energies, 2D density of states and localized wavefunctions, and the SuperLattice (SL) aspect, with strong anisotropy in the Brillouin zone and the resulting small but finite

bandwidth in the direction perpendicular to the layers.
The parameters (choice of the materials, layer thickness, carrier concentration, etc.) that determine the SL or QW character, will be discussed in the next section.

1.1. Superlattices, Quantum Wells & Heterojunctions

The SL periodicity d, superimposed on the lattice periodicity, leads to a division of the original Brillouin zone in subzones, with boundaries at wave vectors $k=n\pi/d$, n being an integer. In the SL direction, i.e. perpendicularly to the layers,the original bulk material bands will be splitted into subbands separated by small bandgaps (minigaps), see fig.3. The width of these subbands and minigaps depends on the SL periodicity and on the potential difference between the constituent layers. Since these subbands are much

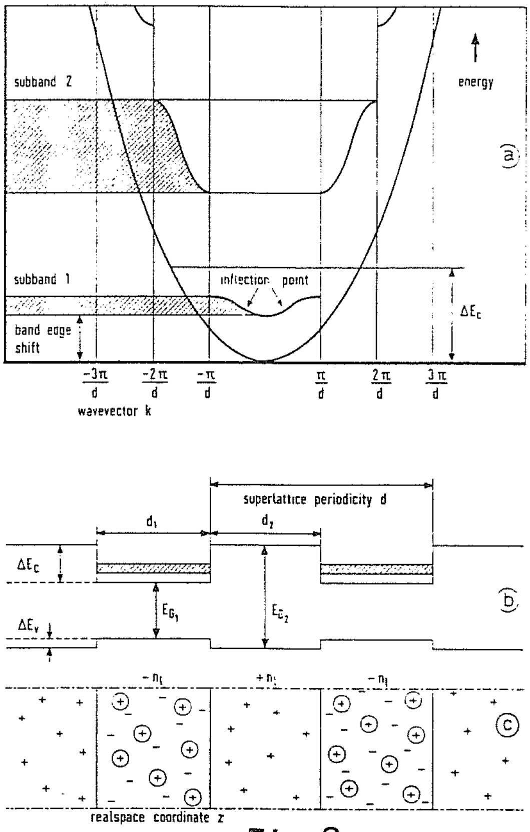

Fig.3

Schematic energy level structure of a type I superlattice. a shows the formation of subbands and the division of the Brillouin zône into subzônes due to the periodic potential ΔE_c. These subbands result from the difference in band gaps of the neighbouring materials as shown in b. c shows the charge distribution in real space for a homogeneously doped superlattice.

narrower than the usual bulk energy bands the inflection point in a band (i.e. where the effective mass changes sign) occurs at much lower energy and smaller k-vectors : therefore it should be possible to accelerate electrons, with an externally applied voltage, up to this inflection point (in bulk materials this is practically impossible since the electron would be scattered by a phonon long before it reaches this point); if this happens the effective mass changes sign and the electrons are slowed down by the field until the mass reverses sign again, etc. :in principle one could thus realize the so-called Bloch oscillator, since in real space the electrons would have an oscillatory motion with a consequent emission of radiation. Furthermore, the average distance travelled by an electron in the tilted conduction band before it is scattered decreases with the increase of the applied voltage; thus an increase of the voltage applied to a SL makes the current flowing through it decrease : the system is said to exhibit a negative differential resistance (this situation is illustrated in Fig.4 ,from Ref. [7]). This fact for example, opens the possibility to use a SL as a rectifier with a very fast response time [8].

Fig. 4

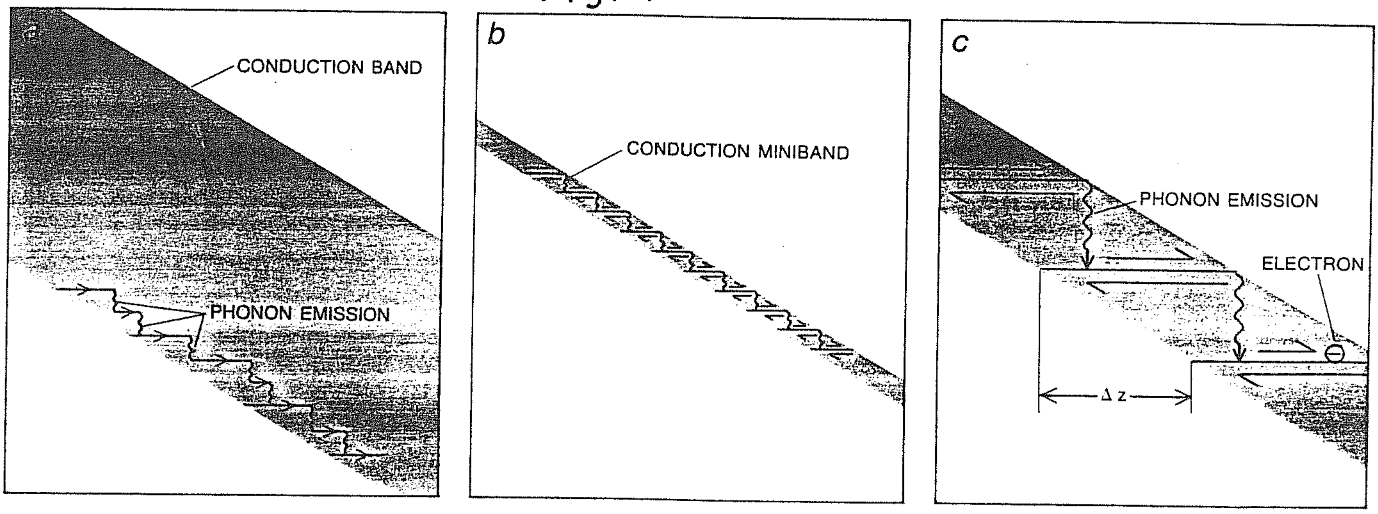

BLOCH OSCILLATION depends on the fact that a voltage accelerates electrons in the conduction band of a semiconductor but at the same time tilts the band. Electrons are therefore propelled toward the upper edge of the band. In a typical semiconductor (*a*) they never arrive. Instead they emit phonons, that is, they excite thermal vibrations in the crystal lattice and "fall" to a lower energy. In a superlattice, where the conduction band is split into narrow minibands, they do arrive. Specifically, they arrive at the upper edge of the lowest conduction miniband (*b*), and on arrival they are reflected. They may oscillate repeatedly between the miniband's edges before they emit a phonon. Since the miniband is tilted, the emission moves the electron's center of mass a certain distance Δz (*c*). That distance decreases with increasing tilt; thus an increase in voltage can have the curious effect of decreasing the current that flows through the crystal.

The electron dynamic in the superlattice direction was analyzed for conduction electrons in narrow subbands [9] : these calculations predicted in fact an unusual current-voltage characteristic including differential negative resistance. The few experimental evidences of such effects ([10] , [11]) were interpreted successfully in terms of the Superlattice effect.

In practice there are fundamental problems that make difficult to see any effect related to the subband width of a SL. To see this we must realize what are the fundamental parameters that determine the SL dimensionality, that is:

a) penetration depth (related to the band structure)

b) mean free path (related to the scattering processes)

c) screening length (related to the charge distribution)

a) The dimensionality (2D or 3D) of a SL can be characterized by the subband width. A flat subband, corresponding to an infinite effective mass, means that successive layers do not interact (Quantum Well case)
A QW is an almost ideal realization of the "particle in a box" model: owing to the confinement of the carriers through the band gap discontinuity, the continuous spectrum of electrons and holes in the direction perpendicular to the layers is split into discrete energy levels and the effective band gap E_g^{eff} increases with decreasing layer thickness (Quantum Size Effect).
The simple "particle in the box" model fails however to describe fully the experimental observations; for example, it neglects excitonic effects which play an important role in these systems: the excitonic binding energy in a thin Ga As layer is significantly higher than that in the bulk material, due to the quasi-two dimensional nature of the exciton.
Furthermore a realistic description of the bulk band structure of the constituent materials must include necessarily band coupling and degeneracies. These facts are important especially for the dispersion relations in the plane of the layers which is not trivial for

states derived from coupled bands such as the p-like valence bands of all III-V semiconducting compounds or the $\vec{k}\cdot\vec{p}$ coupled conduction and valence bands of narrow gap materials. We will address these problems in the II part of this thesis.

The length that characterizes the strength of the interaction between successive layers is the penetration depth of the electron wavefunction of the lower energy material inside the higher energy barriers. If the latters are thin enough, the electrons may tunnel through them into the next well, leading to a finite width of the subbands in the direction parallel to the plane of the layers("real" SL).

For free electron wavefunctions the penetration depth is just the de Broglie wavelength $\lambda = (\hbar^2 / 2m^* V)^{1/2}$, where $\hbar$ is the Planck's constant, m^* the effective mass and V the height of the potential barriers. Typical values for type I-SL are $V \sim 100$ meV, $m^* \sim 0.05m$, leading to the value $\lambda \sim 30$ Å. SL' s with layer thickness of the order of 20 Å can be easily realized by MBE techniques: hence the constraint imposed by the de Broglie wavelength does not prevent the observation of a 3D character SL.

On the contrary, a much more severe constraint is represented by the scattering processes:

b) In order to observe a real SL effect the subband broadening due to scattering must be less than the subband width. This latter, in the case of a 50 Å -SL with a 100 meV potential step, is of the order of 10 meV. The required scattering time can be estimated from the uncertainty relations and is roughly of the order of 10^{-13} sec. Although this time can be easily achieved in a normal semiconductor, in the case of a SL it represents a severe requirement since in order to acquire the necessary energy (say one half of the subband width) from a reasonable electric field (1 KV/cm), the electron must have a mean free path of about 1000 Å or, equivalently, it must traverse 20 layers without being scattered: thus the crystallographic quality of the SL must be excellent, i.e. the constituent

materials must have a very accurate lattice match [1].
Although many materials fulfill the requirement of a precise lattice match (for GaAs/$Ga_{1-x}Al_x$ As systems the lattice mismatch is less than 0.15% at 300° K), the Bloch oscillations have not yet been observed. However, transport measurements have shown tunnelling through multiple barriers and band conduction in the SL direction has been investigated [12].
Recently, magneto-optical experiments on very thin SL in a magnetic field perpendicular to the growth direction have made possible a direct observation of minibands and minigaps [13].In these experiments the electrons, in order to complete their cyclotron orbit, are forced to tunnel through several layers of the SL: the analysis of the intersubband optical transitions allows for a determination of the subband width. Furthermore, these experiments show that even a system composed of only 7 lattice planes of GaAs sandwiched between 2 lattice planes-barriers of GaAlAs still behaves like a superlattice and not as a random alloy of Al atoms in a GaAs matrix.

c) A third fundamental length must be considered when free charges coming from dopant impurities are present :the screening length. For degenerate materials this length is given by the Thomas-Fermi expression $\lambda_{TF}=(E_F \varepsilon /6\pi e^2 n_o)^{1/2}$, where E_F is the Fermi energy, n_o is the net free carrier concentration and ε is the dielectric constant.
For a typical degenerate semiconductor wth $n_o=5\times10^{17}$ cm^{-3} and $\varepsilon=12$, this results in a screening length of the order of 90 Å .
If the layer thickness is much less than λ_{TF}, the charge can be considered as homogeneously distributed over the layer; otherwise the charge will be redistributed across the interface and electrons and holes will accumulate on the two sides of the interface: this situation is typical for heterojunctions. The resulting potential can be calculated by using the Poisson's equation: in general the problem

---

[1] In general, a significant lattice mismatch will be accommodated by the creation of more or less regularly spaced misfit dislocations at the interfaces; these in turn act as traps for free carriers: the resulting localized charge will shield the electric field arising from the potential difference between the layers, thus modifying the energy band line-up.

must be solved self consistently because the charge distribution is the result of the band structure, that in turn depends on the charge distribution itself.

Fig.5 shows schematically the band bending profile resulting from the transfer of charge released from donor or acceptor atoms : in the case represented the heterojunction is made of n-doped GaAs/p-doped GaAlAs. Note the roughly triangular potential well binding the holes and resulting from the ionization of the impurities in the depletion layer.

This system, in contrast to SL and QW, lacks inversion symmetry : this leads to a removal of the Kramer's spin degeneracy (much larger than the one already present in bulk GaAs because of inversion symmetry breaking owing to the difference between Ga and As ionic potentials).

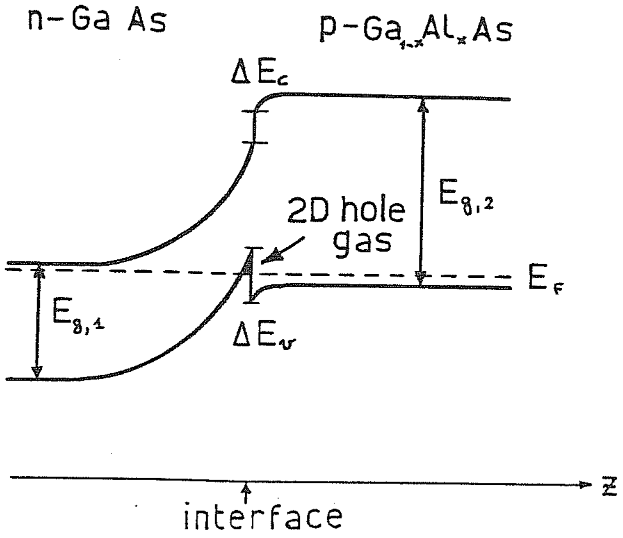

Fig. 5

Energy band profile of a modulation doped heterojunction made of an n-doped GaAs layer grown on a p-doped GaAlAs layer.

Holes are confined near the interface where a 2D hole gas is formed.

z is the coordinate of the growth axis.

1.2. Two-dimensional electrons in Heterostructures : the Quantum Hall Effect

The possibility of realizing two-dimensional systems of electrons or holes either in QW structures or at heterojunction's interfaces, led to the discovery of the Quantum Hall Effect (QHE) : at very low temperature the Hall resistance ρ_{xy} of a 2D electron gas subjected to an intense magnetic field is quantized to values h/ne^2 (where n is an integer), to better than one part in a million [14] ("Normal" QHE).

This quantization, first observed in Si-MOSFET, has been much more extensively studied in GaAs/AlGaAs heterojunctions (see Fig.6) where high electron mobility has been achieved through modulation doping. At still lower temperature and higher magnetic field, an entirely new phenomenon was observed : the quantized plateaus in the Hall resistivity were found at fractional multiples of h/e^2 [15] ("Fractional" QHE).

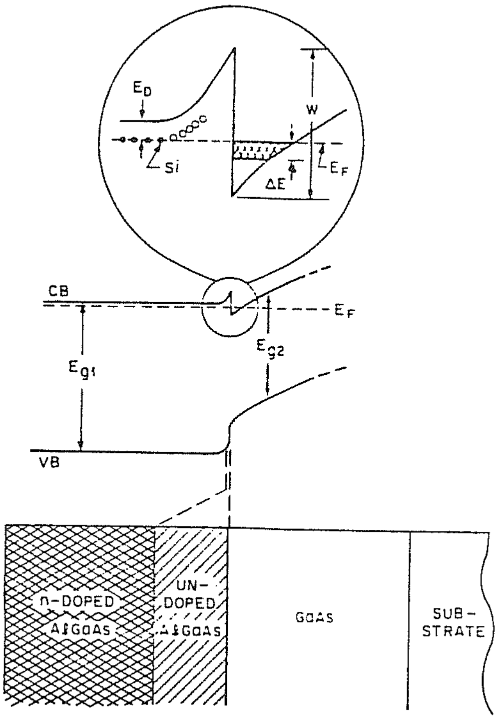

Fig.6

Modulation-doped n-type GaAs$-$Al$_x$Ga$_{1-x}$As heterostructure and its energy band structure. CB and VB refer to conduction band and valence band edges; E_{g1} and E_{g2} are the energy gaps of Al$_x$Ga$_{1-x}$As and GaAs. ΔE is the zero-magnetic-field filling of the two-dimensional electron gas lowest quantum subband, and E_F is the Fermi energy. W is the step height between the GaAs conduction band and the Al$_x$Ga$_{1-x}$As conduction band at the interface

This discovery has spurred a large number of experimental and theoretical studies. A tentative explanation of such fractional filling is based [16] on variational wavefunctions which describes the condensation of a 2D electron gas onto a new state of matter, an incompressible quantum fluid whose elementary excitations are fractionally charged.
For a recent review on QHE, see [17].

1.3. Various types of Superlattices

Hetero-interfaces can be classified roughly into four kinds : type I, type II-staggered, type II-misaligned and type III SL's, as illustrated in Fig.7.b (taken from Ref. [18]).
This classification reflects the different ways in which the bandgap discontinuity $E_{g,1}-E_{g,2}$ is shared between valence and conduction bands.

The most investigated case is that of undoped GaAs/Ga$_{1-x}$Al$_x$As heterostructure where the GaAs bandgap is entirely contained within that of Ga Al As, leading to the square wave modulated potential for

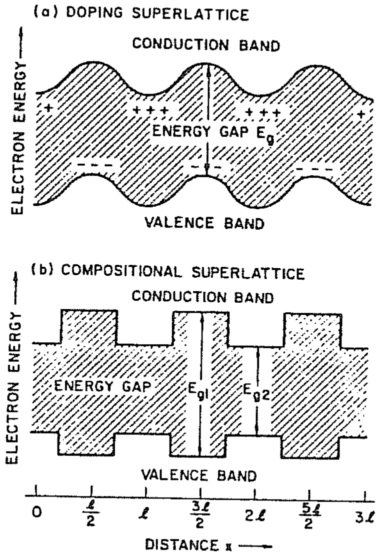

a Spatial variation of the conduction and valence bandedges in two types of superlattices: doping and compositional.

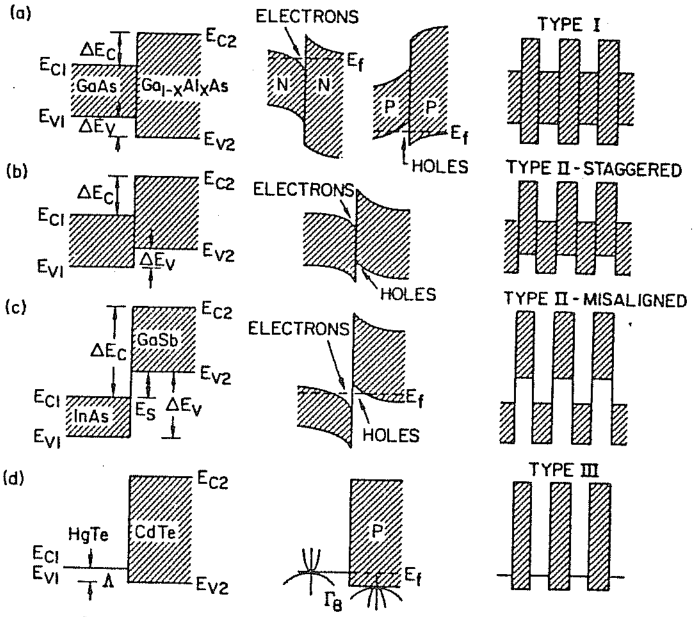

b Discontinuities of bandedge energies at four kinds of hetero-interfaces: band offsets (left), band bending and carrier confinement (middle), and superlattices (right).

Fig.7

the valence and the conduction band schematically shown in fig.7.a. This is an example of type I superlattice.

The so called 'type II-staggered' SL's differs from its type I counterpart by the sign of the band edge discontinuity between the two components of the structure . In this kind of SL, conduction and valence subband wavefunctions are concentrated in different regions: we are thus dealing with an 'indirect band gap in real space'. The spatial separation between electron and hole states reduces the dipole matrix elements for transitions between conduction and valence subbands, thus increasing considerably the radiative electron-hole recombination time.

The binary system InAs/GaSb (type II-misaligned) is characterized by the very unusual band-edge profile shown in fig.7.b: in this case the conduction band edge of InAs is lower in energy than the valence band edge of GaSb, by about 0.15 eV. Charge transfer across the interface is therefore to be expected: experiments show that when the layer thickness reaches a critical value of about 180 Å, a sudden increase in the effective carrier concentration is observed [11].
This transition can easily be understood in a simple double-confinement model ;for thicker layers, electrons (and holes) become less confined and the lowest (highest) subband approaches the bulk band-edge : consequently, at some point the subbands must cross, showing a semiconductor-semimetal transition.
Theoretical calculation [19] based on an EM approach show that actually a small hybridization gap of a few meV opens up at the Fermi energy, producing a very narrow-gap semiconductor rather than a semimetal :the semimetallic behavior observed is probably produced by extrinsic effects .

The unique member of the type III family is the II-VI HgTe/CdTe system (see for example Ref. [20]). where HgTe is a zero-gap semiconductor due to the inversion of the relative position of Γ_6 and Γ_8 edges; the Γ_8 Light Hole band in CdTe becomes the conduction band in HgTe, where their energy difference Λ was determined to be 40 meV.

In a modulation doped superlattice (fig.7a), where the periodic potential is induced by space charge effects resulting from an alternated doping (n-GaAs/p-GaAs, for example) of the same semiconductor compound , the spatial separation between the electrons and their parent donor impurities reduces drastically the Coulomb scattering and thus enhances greatly the mobility of the electrons (peak mobilities of 10^6 cm^2/Vs at 4°K have been achieved, about three orders of magnitude higher than those measured in bulk materials [21]). A recent review on the fundamental properties of Modulation Doped Superlattices is contained in Ref. [22].

1.3.1. Strained Layer Superlattices (SLSL)

The requirement of a nearly perfect lattice match between the constituents of a semiconductor-semiconductor interface can, at certainconditions, be relaxed.

Good superlattices with much more severely mismatched semiconductor materials than, for example , GaAs/AlGaAs, can in fact be grown [23]. For sufficiently thin layers -up to about 300 Å - alternating materials with lattice constants differing by as much as a few percent will accommodate themselves by elastic deformation to a compromise lattice constant . Fig.8 shows schematically that there exists a critical value t_c for the thickness of an epitaxial layer grown on a lattice-mismatched substrate that separates the regime of dislocation formation from that of elastic deformation.

Such "Strained - Layer" SL come out to be astonishingly free of the interface dislocations that would have destroyed those optical and electrical properties that are desirable in a SL. In particular, theoretical and experimental analysis of SLSL made of mismatched ($\delta a/a \gtrsim 1\%$) ternary compounds such as $In_xGa_{1-x}As$ or $GaAs_xP_{1-x}$,indicate that by varying their layer thickness and composition one can vary, continuously and independently of one another, the lattice constants, the forbidden energy gap and the transverse carrier mobility

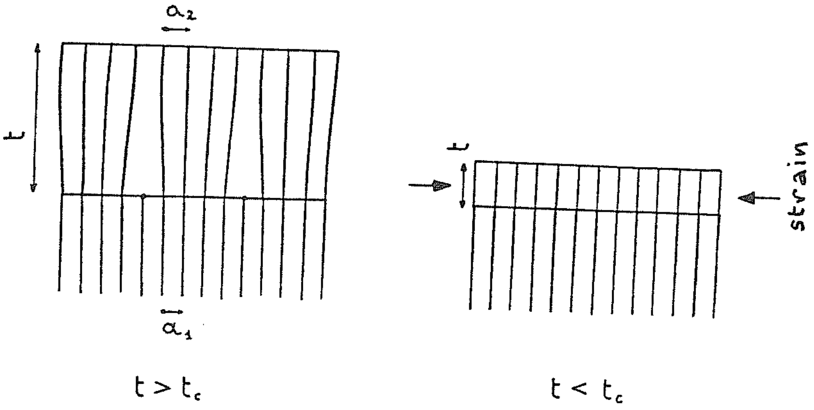

Fig.8

of the overall SL [24].

Recently, optical absorption measurements in GaSb/AlSb SLSL have also shown a reversal of the Heavy Hole and Light Hole exciton peak position :the ground valence state in these structures is the LH level [25]. This effect can be understood by noting that : (i) a biaxial tensile stress resulting from the lattice mismatch, acts on the GaSb layer, that is stretched in the (x,y) direction of the layer plane ; (ii) as a result of this strain there is a removal of the degeneracy of Light and Heavy hole valence bands at $\vec{k}=0$ (see fig.9).

These facts, together with the competing splitting of valence bands due to the quantum confinement , are responsible for the observed unusual behavior. Another consequence of this elastic deformation in GaSb/AlSb system is an observed band-gap shrinkage of

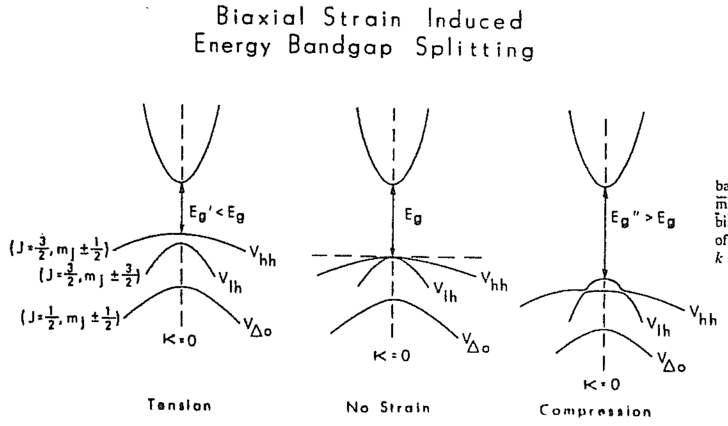

Fig. 9

Representations of the energy-band-gap splittings and shifts caused by mismatch strain in the epitaxial layer. The biaxial shear strain breaks the degeneracy of light- and heavy-hole valence bands at $k = 0$.

J. Appl. Phys. 57 (12), 15 June 1985

about 50 meV .

1.4. Band offset in GaAs/Al Ga As heterostructures.

An extremely important input parameter for the calculation of energy levels in heterostructures is the band gap discontinuity, i.e. the relative energy position between the conduction band edges of the two constituent materials (see Fig.10). This parameter determines the height of the barriers confining the particles in the quantum wells and thus controls the distribution and flow of mobile carriers. In spite of its central role this quantity is not accurately known, even for extensively investigated systems like GaAs/Ga Al As.

As can be seen in fig.10, the published experimental values of $Q_c = \Delta E_c/\Delta E_g$ are quite scattered even in recent years, ranging from the 85% of the earliest determination [26] to the more recent 60% [27] . The experiments do not seem to indicate any relevant dependence of Q_c on the Al concentration x.

The most accurate estimate, based on anelastic light scattering by photoexcited electrons , gave $Q_c = 0.69 \pm .03$ (x=.06) [28] : this method doesn't suffer from the large amount of uncertainty usually present in optical determination of band-offset (primarily because

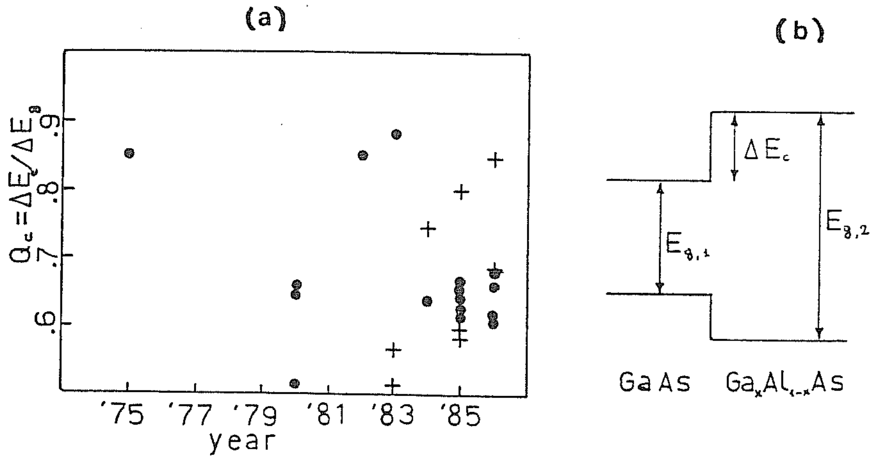

Experimental determinations of the conduction-band discontinuity $Q_c = \Delta E_c/(E_{g,2}-E_{g,1})$ vs. year. ● and + mean that optical and electrical methods respectively, have been used.

Fig.10

of the complicated valence band structure and of excitonic effects) since it involves only electronic subbands . Also, it allows a direct measurement of the total discontinuity $\Delta E = E_{g,1} - E_{g,2}$, so that an exact knowledge of the alloy composition x is no longer needed. Theoretical predictions can hardly be of any help, given the normal uncertainty ($\gtrsim 0.1$ eV) of the best band calculations in bulk materials. Moreover, the oldest and simplest model used to predict semiconductor - semiconductor band lineup, based on the assumption that the conduction band discontinuity Q_c is simply equal to the difference between the electron affinities of the two materials, has proven to be incorrect [29].

CHAPTER II

THE ENVELOPE-FUNCTION APPROXIMATION

2. The Envelope Function Approximation

An approach to the description of electronic states in semiconductor heterostructures that has proved to be simple, versatile and accurate is based on the "Envelope Function" method ([30] , [31]). It is instructive to discuss briefly the motion of electrons and holes in a semiconductor characterized by simple, isotropic ,non-degenerate conduction and valence bands with an extremum at $\vec{k}=0$, in the scheme provided by the Effective Mass (EM) theory, and then consider the problem of imposing the appropriate boundary conditions on the envelope function at a sharp interface between two different semiconductors.

The approach to the more complex problem involving degenerate bands will be treated in Paragraphs 2.3 and in APPENDIX G.

2.1. The Effective Mass Equation

We will quote only the main results of EM theory in a simple one band case (a detailed derivation is contained in APPENDIX A). Consider the motion of an electron in a semiconductor ,in the presence of some additional potential $U(\vec{r})$;the Schrodinger equation is:

$$[\ p^2/2m + V_c(\vec{r}) + U(\vec{r}) - E\ ]\ \Psi(\vec{r}) = 0 \qquad (2.1)$$

For example, $U(\vec{r})$ could be the band-bending potential on the right side of the interface depicted schematically in Fig.5. If the additional potential is slowly varying and weak, the wave function Ψ is approximately given by the $\vec{k}\cdot\vec{p}$ expansion (see APPENDIX B for a detailed derivation) :

$$\Psi(\vec{r}) = F(\vec{r})u_{n0}(\vec{r}) + (1/m)\sum_{n'\neq n} \frac{-i[\vec{\nabla}F(\vec{r})]\cdot\vec{p}_{n'n}}{E_n(0) - E_{n'}(0)}\, u_{n'0}(\vec{r}) \qquad (2.2)$$

Eqn.(2.2) shows that to lowest order $\Psi(\vec{r})$ is given by a slowly varying "envelope " function $F(\vec{r})$ modulating the rapidly varying Bloch part $u_{n0}(\vec{r})$. The second term is a correction arising from the coupling with other bands, as it is obtained in the $\vec{k}\cdot\vec{p}$ method .

The envelope function $F(\vec{r})$ satisfies the Effective Mass Equation (A.17), that is :

$$[\ -(\hbar^2/2m^*)\nabla^2 + U(\vec{r})\ ]\ F(\vec{r}) = [\ E - E_n(0)\ ]\ F(\vec{r}) \qquad (2.3)$$

The energy E of the electron, in the case of a simple,isotropic band extremum (e.g. the conduction band minimum in GaAs semiconductor) is given by :

$$E_n(\vec{k}) = E_n(0) + \hbar^2 k^2/2m^* \qquad (2.4a)$$

where

$$1/m^* = 1/m + (2/m^2)\sum_{n'\neq n} \frac{p^{\alpha}_{nn'}p^{\alpha}_{n'n}}{E_n(0) - E_{n'}(0)} \quad ,\ \alpha = x \text{ or } y \text{ or } z \qquad (2.4b)$$

2.2. Boundary conditions for the Envelope Function.

In the EM equation (2.3) for the envelope function, all reference to the microscopic structure of the host semiconductor is condensed in the effective mass m^* and the band edge energy $E_n(0)$. These two parameters assume different values in the two semiconductors, say A and B, making up an interface system.

Thus one could think of writing a more general form of the eqn.(2.3), in which the effective mass and the band edge vary as a function of z, the coordinate of the axis perpendicular to the interface.

$$\{-(\hbar^2/2)\,\vec{\nabla}\cdot(1/m^*(z)\,\vec{\nabla}\ )\}\ F(\vec{r}) = \{E - E_n(0,z) - U(r)\}\ F(r) \qquad (2.5)$$

(z=0 represents the interface plane). The kinetic energy term in the first member has been written in a way that restores the hermitean character of the EM Hamiltonian .

Typically, the transition region include only a few atomic layers : the potential term in eqn.(2.5) is thus rapidly varying near the interface, contrarily to the fundamental assumption of the EM theory, and the whole EM formalism becomes questionable. Nevertheless, it is possible to provide the EM equation with boundary conditions that makes it useful also in the case of abrupt junctions, by means of the following argument.

Assume that an abrupt heterojunction is located at $z=0$. Then for $z<0$, $m^*=m_A^*$ and $E_n(0) = E_n^A(0)$; for $z>0$ $m^*=m_B^*$ and $E_n(0) = E_n^B(0)$. One now imposes the reasonable requirement that $F(z)$ be finite everywhere : thus the right-hand side of eqn. (2.5) is finite, having only a finite discontinuity at the interface. The left-hand side must be similarly well behaved; this implies

$$d/dz(1/m^*)dF/dz \text{ is finite for all } z \qquad (2.6)$$

By integrating the preceding expression between $z=-\varepsilon$ and $z=+\varepsilon$ and taking the limit $\varepsilon \longrightarrow 0$ one is lead to the conclusion (first derived in Ref.[30]) :

$$(1/m_A^*)dF^A/dz\Big|_{-\varepsilon} = (1/m_B^*)dF^B/dz\Big|_{+\varepsilon} \qquad (2.7)$$

The existence of stationary states (probability density constant in time) implies that the z-component of the current be the same on all planes parallel to the interface and therefore also that its average over a microscopic volume Ω, including one or few unit cells, be the same on both sides of the interface. One finds, for the average current $\bar{J}$ in A-material :

$$\bar{J}_A = (\hbar/m)\ \mathrm{Im}\int_\Omega \Psi_A^* \frac{\partial}{\partial z}\Psi_A\, d\vec{r} = (\hbar/m_A^*)\ \mathrm{Im}\ \{\ F^{A*}(0)\frac{\partial}{\partial z}F^A(0)\ \} \qquad (2.8)$$

Therefore the continuity of $\bar{J}$ implies :

$$(\hbar/m_A^*)\ \mathrm{Im}\ \{\ F^{A*}(0)\frac{\partial}{\partial z}F^A(0)\ \} = (\hbar/m_B^*)\ \mathrm{Im}\ \{\ F^{B*}(0)\,\partial/\partial z\,F^B(0\ \} \qquad (2.9)$$

One can see that from the condition (2.7), together with the requirement that $F(z)$ be continuous across the junction :

$$F^A(0^-) = F^B(0^+) \qquad (2.10)$$

it follows that the current $\bar{J}(z)$ is continuous across the interface. It is easy to show furthermore that the Hamiltonian appearing in eqn.(2.5) is consistent with the conserved current $\bar{J}(z)$,that is the usual continuity equation holds for the probability density $F^{i*}F^{i}$ in each material:

$$d|F^{i}|^{2}/dt + d\bar{J}_{i}(z)/dz = 0 \quad , \qquad i=A,B \ . \qquad (2.11)$$

It is now clear that the boundary conditions (2.7,2.10) on the envelope function imply that the average of the probability current is constant. They are, therefore, significant on physical grounds and can be safely adopted in the treatment of heterostructures.

From the condition (2.10), the continuity of the total wavefunction (2.2) implies [2]

$$u_{n}^{A} \cong u_{n}^{B} \qquad (2.12)$$

(We drop, from now on, the subscript '0' in the Bloch part of the wavefunction).
The preceding equation is plausible, given the structural similarities of the III-V compounds, as long as one is considering the same band edge on both side of the interface.

Finally, it is interesting to note that kinetic energy operators such as

$$[\ 1/m^{*}\hat{p}^{2} + \hat{p}^{2}\,1/m^{*}]/4$$

that seem reasonable a priori, are not acceptable in treating abrupt heterojunctions within the Envelope-Function scheme, since in this case the plane z=0 acts as an impenetrable barrier and the current $\bar{J}(z)$ is no longer conserved [32].

2.3. Coupled bands.

The simple band approach that has been outlined in the previous paragraphs cannot be used in practice in many situations of interest. This may happen because of :

a) Band degeneracy near an extremum, as in the valence band maximum

---

[2] It is also assumed that the second term in the wavefunction (2.2) is small.

at Γ in all cubic semiconductors.

b) Coupling between bands that produces deviations from parabolicity, as in the conduction band of direct gap semiconductors.

In the case of GaAs, which is of interest here, this non parabolicity has a sizeable effect on levels with energy $\gtrsim$ 100 meV above the band minimum: since this energy is comparable with the confinement energy of an electron in a typical superlattice, this effect cannot be neglected.

Let's consider explicitly the case of the III-V compound GaAs.
In Fig.11.a we show the calculated energy bands for GaAs, with the inclusion of spin-orbit interaction (from Ref.[53]). The top of the valence band is at $\vec{k}=0$; the non-relativistic bands are six-fold degenerate (including the spin degeneracy) at Γ point, with symmetry Γ_{15} (p-like orbitals). The additional spin-orbit interaction couples operators in spin space and ordinary space and thus reduce the symmetry : the Γ_{15} states are split into Γ_7 and Γ_8 states (fig.11.b); the upper manifold is four-fold degenerate and can be

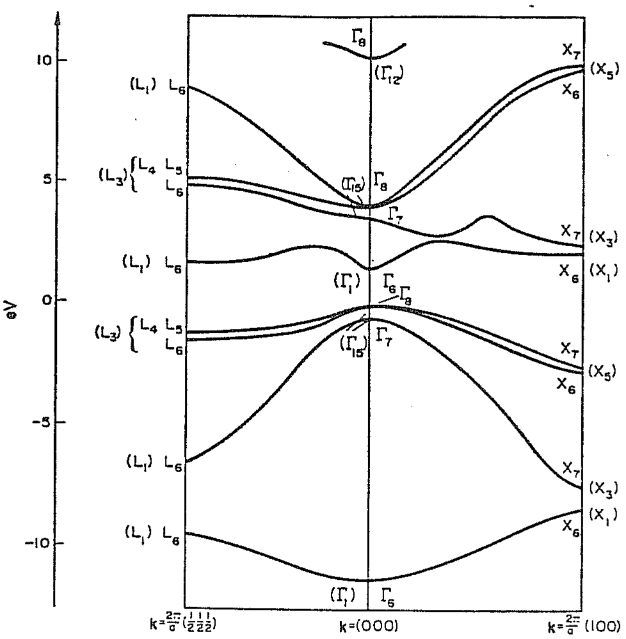

Energy bands for GaAs with the inclusion of spin-orbit interaction. The irreducible representations for the states of the simple group are supplied in brackets.

Fig. 11.a

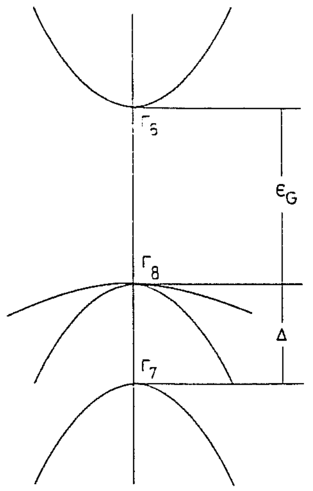

Fig.11.b A schematic illustration of the band structure in III-V semiconductors near the Γ point. Γ_6 is the conduction band, Γ_8 gives the heavy and light holes, and Γ_7 is called the spin-splitoff band.

classified with the total angular momentum quantum number J=3/2, the four states thus corresponding to J_z =±1/2,±3/2 ;the Γ_7 states are two-fold degenerate and correspond to J =1/2. The spin-orbit interaction is very important in narrow-gap semiconductors, where it produces valence band splittings as big as the main gap.
In the case of GaAs, the splitting Δ is found to be 0.341 eV, while the value of the energy gap is E_g =1.519 eV (at 4°K).
Even if we regard the interaction between states Γ_7 and Γ_8 as being very small, we still have a degenerate problem and we must include the interaction between the two bands that go into Γ_8 at $\vec{k}=0$. The problem is to derive an extended version of the Effective Mass equation (A.17) in this case : one cannot use the simple procedure of APPENDIX A (eqns. (A.12) to (A.17)) since the band structure is not a single valued function of $\vec{k}$ and cannot be simply written as a Taylor expansion.

It can be shown [33] that, in a standard second order $\vec{k}\cdot\vec{p}$ description of a set of coupled band edges at the point of a direct gap semiconductor, the band structure at a given $\vec{k}$-value is given by the eigenvalues of an NxN matrix :

$$H_{ij}(\vec{k}) = \sum_{\alpha,\beta} D_{ij}^{\alpha\beta} k_\alpha k_\beta + \sum_\alpha P_{ij}^\alpha k_\alpha + E_i \delta_{ij} \quad (i,j=1,2..,N) \qquad (2.13)$$

where α,β run over x,y and z and N is the number of bulk bands that contribute with comparable weight to the formation of the wavefunctions. The terms $P_{ij}^\alpha k_\alpha$ in eqn.(2.13), where the matrix P^α is given by $P_{ij}^\alpha = \hbar/m\langle u_i | p_\alpha | u_j \rangle$, represent the first order direct $\vec{k}\cdot\vec{p}$ interactions between the N bands, while the quadratic terms proportional to the matrix $D^{\alpha\beta}$ represent the indirect $\vec{k}\cdot\vec{p}$ coupling between two of the N bands via the other bands not included explicitly in the set. The form of the matrix depends on the choice of the unperturbed functions at $k=\vec{0}$.

To give a specific example, consider the 6x6 matrix given in the APPENDIX D (atomic units ,in which $\hbar$ = m = 1,are used in the APPENDIX and will be used in the text from now on) , which represents the conduction band and the upper spin-orbit split component of the valence band (Γ_6 and Γ_8 states in Fig.11.b) : this matrix is known to give a very accurate description of these bands near $\vec{k}=0$ for materials with large spin-orbit splittings . One has a conduction band with s-like character at Γ_6 and two spin states $s\uparrow$ and $s\downarrow$. The parameter P is defined in terms of the interband momentum matrix element

$$P = -i \langle s|p_x|x\rangle \qquad (2.14)$$

where $|x\rangle$ indicates the valence band state that transforms as an atomic P_x -like function under the symmetry operations of the cubic group and $|s\rangle$ indicates the conduction wavefunction at Γ_6.
The effective mass m^* appearing in the corresponding diagonal terms originates from the coupling to the bands not included in the set, and primarily from the split-off valence band .
One finds [34] :
$m^{*-1} = 1 + 2P^2/3(E_c - E_v + \Delta)$, where Δ is the valence band spin-orbit splitting and E_c ,E_v are the conduction and valence band edges at point. Δ is given explicitly by the following expression [33] :

$$\Delta = (3i/4c^2)\ \langle x|(\partial V_c/\partial x)p_y - (\partial V/\partial y)p_x|y\rangle \qquad (2.15)$$

where V_c is the periodic crystal potential.
The basis set used consists of the (J,J_z) functions for a total angular momentum J = 3/2 [35] :

$$u_1 = |s\uparrow\rangle$$
$$u_2 = |3/2;\ 3/2\rangle = |1/\sqrt{2}\ (x+iy)\uparrow\rangle$$
$$u_3 = |3/2;-1/2\rangle = |-1/\sqrt{6}\ (x-iy)\uparrow - \sqrt{2/3}\ z\downarrow\rangle$$
$$(2.16)$$
$$u_4 = |s\downarrow\rangle$$
$$u_5 = |3/2;\ 1/2\rangle = |-\sqrt{2/3}\ z\uparrow + 1/\sqrt{6}\ (x+iy)\downarrow\rangle$$
$$u_6 = |3/2;-3/2\rangle = |-\sqrt{1/2}\ (x-iy)\downarrow\rangle$$

where $|x\rangle$, $|y\rangle$, $|z\rangle$ are valence p-like band states and the symbols $\uparrow$ and $\downarrow$ denote the spin "up" and "down" states respectively.

If one wishes to consider the energy region close to the valence band top, then the conduction band can be ignored altogether , i.e. one removes rows and columns 1 and 4 in the matrix (D.1) (and renormalize the values of γ_1, γ_2, γ_3 and K as described in APPENDIX F). The resulting 4x4 matrix is the well-known Luttinger Hamiltonian [36] describing the light and heavy hole bands in cubic semiconductor (see (3.3),(3.4)).

The parameters $\gamma_1, \gamma_2, \gamma_3, K$ and P are specific of each material and represent, together with the band edges positions E_j ,the only input parameters required for the energy band calculation in an EM Theory. Usually they are determined experimentally by fitting cyclotron resonance data :their values for GaAs and AlAs are listed in APPENDIX F, those of $Al_xGa_{1-x}As$ following by linear interpolation. The energy-gap difference between GaAs and Al Ga As, in the region $x \lesssim 0.45$ where the $Al_xGa_{1-x}As$ alloy has a direct gap, can be expressed as [37]:

$$E_g(x) = E_g(GaAs) + 1.155\ x + 0.37\ x^2 \qquad (2.17)$$

Here $E_g(GaAs) = 1.519$ eV is the value of the band gap at 4°K.

The extension of the EM eqn.(2.3) to the many-band case, in analogy with the many-band EM equation used in the theory of acceptor impurities [38] , is represented by the following system of N differential coupled equations [31]

$$\sum_{j=1}^{N} \{ H_{ij}(-i\vec{\nabla}) + U(\vec{r})\,\delta_{ij} \} F_j(\vec{r}) = E\ F_i(\vec{r}) \qquad (2.18)$$

for the N-component envelope-function $F_i(\vec{r})$, i=1,2,..,N; H_{ij} is the Hamiltonian matrix (2.13). The total wavefunction $\Psi(\vec{r})$ is expressed, in analogy with eqn.(2.2),as

$$\Psi(\vec{r}) = \sum_j \{ F_j(\vec{r}) u_j(\vec{r}) + \sum_{j'>N} \frac{-i[\vec{\nabla} F_j(\vec{r})]\cdot\vec{p}_{j'j}}{m\{E_j(0) - E_{j'}(0)\}} u_{j'}(\vec{r}) \} \qquad (2.19)$$

The second term represents a correction (to first order in $\vec{k}\cdot\vec{p}$) due to higher bands and can, for many purposes, be neglected.

We note in eqn.(2.16) that the kinetic energy part is just obtained by replacing $\vec{k}$ with $-i\vec{\nabla}$ in the $\vec{k}\cdot\vec{p}$ matrix, and that the potential energy term is diagonal in the band index ;this is a consequence of its slow spatial variation :as it can be taken as a constant in each unit cell, its off-diagonal matrix elements vanish by Bloch function orthogonality.

The generalization of the boundary conditions (2.7),(2.10) in the many-band case is quite straightforward and is discussed briefly in APPENDIX G.

2.4. Effective Mass vs. Tight-binding Theories.

In the EM approximation the superlattice wavefunction is written as a linear combination of Brillouin zone-center bulk states, with a slowly varying envelope modulation along the SL axis. Although Envelope-function calculations are found to be in very good overall agreement with experiments, there are specific situation where a more complete description is needed.
This can occur when two or more bulk states with widely separated wave vectors contribute significantly to a given SL state. An example occurs in the SL subbands above the lowest conduction subband in the GaAs/AlGaAs - SL. As the subband energies approach the GaAs X-point conduction band minimum (see the band structure in Fig.11.a), the SL states become a mixture of Γ -point and X-point related bulk states. Since the Envelope Function method is based on a single $\vec{k}$-point bulk states only (the Γ -point in the present case),this X-point contribution is omitted.

A second example can occur in SL valence bands. The Envelope-Function approximation allows no mixing of bulk HH and LH states in the SL wavefunction at the BZ-center (This is immediately apparent from the expression of the Hamiltonian (D.1) when $k_x = k_y = k_z = 0$).
This approximation is realistic as long as the HH and LH states are sufficiently separated in energy. However, for certain layer thickness and barrier alloy concentration, they can be close to one another. For example, in a GaAs QW between $Al_xGa_{1-x}As$ barriers, with x=0.25 and assuming that the valence band discontinuity is 40% of the total band-gap discontinuity, a crossover between the first LH and the second HH subbands is expected when the GaAs layer thickness

is about 280 Å.
This $\vec{k}=0$ mixing can have a substantial effect on optical and transport properties, since they depend mainly on the band structure near the zone-center.
A surprisingly large (~30%) admixture of the LH states in the highest Heavy hole subband state in a 210 Å - GaAs/AlGaAs QW structure was found at $\vec{k}=0$ by investigating the polarization of the optical emission spectra [89]. Attempts to interpret these results within the Effective Mass approximation and coupling with Luttinger Hamiltonian yield quantitative disagreement: several other coupling mechanism (strains in the layers, electric fields, asymmetry in the Quantum Well), were found to be inadequate as well.

An alternative approach to the EM one consists in the use of empirical Tight-Binding models, in which the SL wavefunction is described as a linear combination of atomic-like orbitals.
Tight-Binding calculations have been performed on InAs/GaSb and GaAs/AlGaAs SL [42] : although in most cases the Γ-point states are found to be predominant, a certain admixture of other bulk states seems necessary in order to describe correctly the aforementioned particular situations.
A drawback of TB methods is that they lead to big-sized problems when they are applied to thick SL's, since the dimension of the Hamiltonian matrix increases with the size of the repeated unit cell.
Moreover, the implementation of self-consistent calculations when charge transfer in the heterostructure is expected, is somewhat difficult in a Tight Binding approach.

2.5. Inclusion of an external magnetic field:Landau levels in Heterostructures

One of the main advantages of the Envelope-Function method is that it can be easily extended to include external fields. Here we shall discuss the effect of an external magnetic field applied perpendicularly to the layers constituting the heterostructure.

Many of the most revealing experiments on 2D systems are performed in an external magnetic field : the reason is that in a two-dimensional system - for example electrons or holes in an isolated QW or in the binding potential at the interface of a doped heterojunction (Fig.5,6) - a perpendicular magnetic field quantizes both available degrees of freedom, producing an entirely discrete spectrum and thus leading to an enrichment of optical structures and also to new transport phenomena, like the Quantum Hall Effect .

The inclusion of a magnetic field in the Envelope function formalism can be accomplished in the following way [39]:
the field $\vec{B}=(0,0,B)$ is described by the vector potential $\vec{A}$ (it is convenient to choose the gauge with $A_z=0$). In the $\vec{k}\cdot\vec{p}$ bulk Hamiltonian, $\vec{k}$ is to be replaced by $\vec{k}' = \vec{k} + (e/c)\vec{A}$. Since the components of $\vec{k}'$ doesn't commute :

$$[k'_x, k'_y] = -i(e/c)B \qquad (2.20)$$

one must go back to the original Luttinger-Kohn Hamiltonian, [36] written in term of the anticommutators $\{k_i, k_j\}$,to derive the correct expression when a magnetic field is present.
Also , new diagonal terms arise, representing the direct coupling of the electron and hole to the field ; the conduction band diagonal terms in the 6x6 Hamiltonian (D.1) now become :

$$H_{cc} = E_c + (\vec{k} + e\vec{A}/c)^2 /2m^* + (e/2cm)g^* s_z B \qquad (2.21)$$

where $\vec{s}$ is the electron spin ($s_z=\pm 1/2$) and the effective g-factor is written, following Roth et al. [34] , as :

$$g^* = 2m/m^* \qquad (2.22)$$

For the valence band diagonal elements, one must add the terms :

$$(e/c)\kappa J_z B + (e/c)q J_z^3 B \qquad (2.23)$$

where J_z is the spin 3/2 matrix operator and κ, q are two material parameters [38]. Actually q is very small for the semiconductors of interest here and will be set to zero.

As a consequence of (2.20), one can define operators a, a^+:

$$a = (c/2eB)^{1/2}(k'_x - ik'_y) \quad , \quad a^+ = (c/2eB)^{1/2}(k'_x + ik'_y) \qquad (2.24)$$

obeying the commutation relation $[a,a^+]=1$. Thus all terms in k_x, k_y in the Hamiltonian can be expressed in terms of these harmonic oscillator raising and lowering operators.

It is possible to write a closed-form solution of the eigenvalue problem only if one takes the axial approximation. In fact, the full Hamiltonian can be written as :

$$H = H_{axial} + H_{cub} \qquad (2.25)$$

Part of the anisotropy in the (k_x, k_y) plane is included in the H_{axial} part which has axial symmetry and can be solved exactly. The other term H_{cub} ,which is neglected in the axial approximation ,has the form :

$$H_{cub} = \begin{vmatrix} H_a & 0 \\ 0 & H_b \end{vmatrix} \quad , \text{ where } \quad H_a = H_b \equiv A \begin{vmatrix} 0 & 0 & 0 \\ 0 & 0 & a^{+2} \\ 0 & a^2 & 0 \end{vmatrix} \qquad (2.26,27)$$

and

$$A = \sqrt{3}\,\hbar eB/2cm\ (\gamma_2 - \gamma_3) \qquad (2.28)$$

Inclusion of the anisotropic term proportional to $\mu = (\gamma_2 - \gamma_3)/2$ uncrosses some of the Landau levels but the absolute shifts are always less than 10% [51] .

In particular, Landau levels with n and n±4 are coupled by the μ-term. This implies that ,for example, the levels with n=-1 and n=3 in Fig.31 should not cross and that those two levels actually have mixed n=-1 and 3 character.

Since the effect of this "warping" term is small (see also in APPENDIX H of this thesis), we will assume $H_{cub} = 0$. In this case one can see by inspection that the solution in each material of the eigenvalue problem associated with H takes the form :

$$F_n = (c_1(z)\varphi_n, c_2(z)\varphi_{n-1}, c_3(z)\varphi_{n+1}, c_4(z)\varphi_{n+1}, c_5(z)\varphi_n, c_6(z)\varphi_{n+2})$$
(2.29)

where the $\varphi_n(x,y)$ are the harmonic oscillator wave functions with

$n = -2, -1, 0, \ldots$ and the c_j coefficients are automatically vanishing for the components with negative oscillator index.
If one lets the a , a^+ operators act on the state (2.29), finds that the effective Hamiltonian in the axial approximation takes the form :

$$H_{jj'} = (D^{z}_{jj'} k_z^2 + E_j)\,\delta_{jj'} + (P^{z}_{jj'} + A_{jj'}(n,B))k_z + C_{jj'}(n,B) \qquad (2.30)$$

where j, j' run over the 6 basis states and A, C matrices represent the magnetic field induced terms. The explicit expression of $H_{jj'}$ is contained in APPENDIX E.

With the replacement $k_z = -i\,\partial/\partial z$ in (2.30), the Effective Mass equation $\sum_{j'} H_{jj'} F_{j'} = E\ F_j$ becomes a system of differential equations for the envelope functions $c_j\ (z)$.
The following conditions must be imposed in order to satisfy the boundary conditions [39] :

$$-iD^{zz}_{jj} \frac{\partial}{\partial z} c_j(z) + (1/2)\sum_{j'} A_{jj'}\, c_{j'}(z) \qquad \text{continuous for} \quad j=1,\ldots,6$$
(2.31)

For the superlattice case, all six $c_j(z)$ functions have the common prefactor $\exp(ik_{sz}\ z)$, where k_{sz} is a quasi-momentum in the SL-Brillouin zone. For SL with very thick barriers (QW limit), the latter dependence is very small and can be neglected.

CHAPTER III

SUBBANDS IN QUANTUM WELLS AND SUPERLATTICES

3.1. Two-dimensional subbands in Semiconductor Heterostructures.

In a SL one has a very thin Brillouin zone in the K_z-direction [3] of width $2\pi/d$ (d being the SL period) and one of the usual size $2\pi/a$ in the k_x, k_y direction (a being the lattice constant). One is dealing, therefore, with a very asymmetric band structure with a bulk-like band width ($\sim$10 eV) in the k_x, k_y plane and narrow ($\sim$10 meV) bands in the k_z -direction.
Let's go back to the $\vec{k}\cdot\vec{p}$ matrix (D.1).
The dispersion in the k_z direction is relatively simple to handle, since most of the diagonal terms in the matrix vanish for $k_x, k_y = 0$.
In particular one sees that the $J_z = \pm 3/2$ states, corresponding to the Heavy Holes (HH), completely decouple from the other bands ;their dispersion is purely parabolic, with an effective mass :

$$m_H^*/m = (\gamma_1 - 2\gamma_2)^{-1} \qquad (3.1)$$

In a superlattice geometry one thus has a Kronig-Penney type of eigenvalue problem, with the boundary conditions (2.7),(2.10). The dispersion relation can be found analytically and is given implicitly by the following equation [30]

$$\cos(k_z d) = \cos(k_{zA} d_A)\cos(k_{zB} d_B) - $$
$$-(1/2)(m_H^A\, k_{zB}/m_H^B\, k_{zA} + m_H^B\, k_{zA}/m_H^A\, k_{zB})\sin(k_{zA} d_A)\sin(k_{zB} d_B)$$

(3.2)

where $k^2_{zA,B} = 2m_H^{A,B}(E - E_V^{A,B})$ and d_A, d_B are the thickness of the A and B layer respectively. As for Light Holes (LH) and conduction electrons, one still has a 2x2 matrix between $s\uparrow$ and $J_z = +1/2$ (and an equivalent one for $s\downarrow$ and $J_z = -1/2$).

---

[3] We assume that the growth axis of an MBE heterostructure is in the <001> direction ,as it usually is .

Consider now the dispersion for $k_x, k_y \neq 0$. It has been shown [39] that the coupling between HH and LH states via the Luttinger Hamiltonian matrix elements, together with the requirements imposed by the SL boundary conditions, results in strong non-parabolic dispersion of the subbands in the plane (k_x, k_y).
In Fig.12 results for a 120 Å QW of GaAs sandwiched between $Al_xGa_{1-x}As$ barriers with x=0.21 are shown : they are obtained [43] in the many-band Envelope-Function model just described ,with the appropriate boundary conditions . It has been assumed that the con-

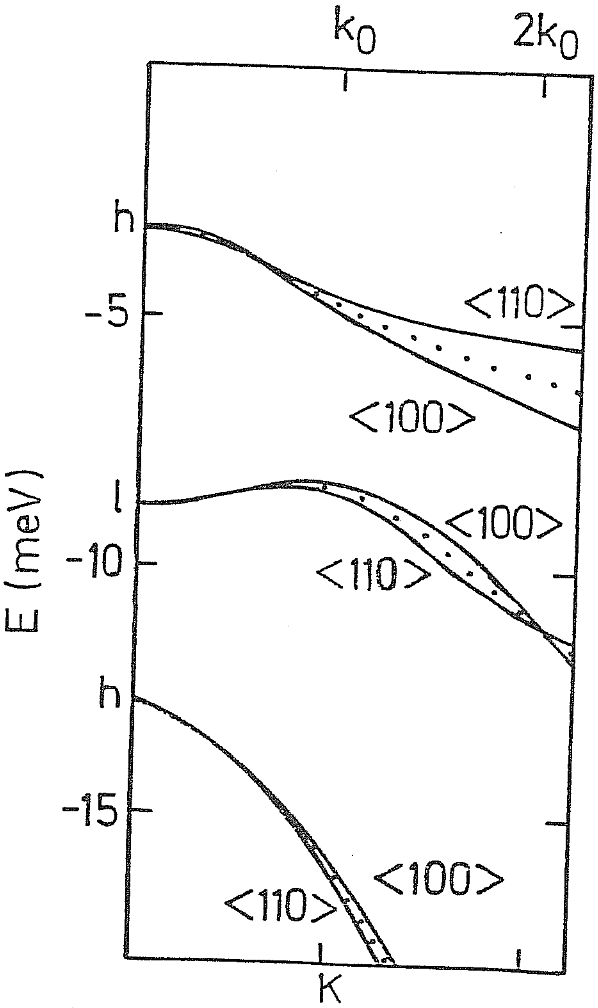

Fig. 12

Dispersion of valence subbands of a 140Å GaAs - 200Å $Al_xGa_{1-x}As$ superlattice, with x = 0.21, in the plane perpendicular to the <001> growth axis. Solid lines: dispersion for $\vec{k}$ in the <100> or <110> directions. Dotted line: axial approximation. k_0 denotes $\pi/340Å = 9.24 \cdot 10^5$ cm^{-1}. h and l denote "heavy" or "light" character at $\vec{k}$ = 0.

duction bands are decoupled, so that the hole states are described by the well-known Luttinger-Kohn Hamiltonian :

$$\hat{H} = E_v \hat{I} + \hbar^2/2m \left| \begin{array}{cccc} A_+ & B & C & 0 \\ B^* & A_- & 0 & C \\ C^* & 0 & A_- & -B \\ 0 & C^* & -B^* & A_+ \end{array} \right| \qquad (3.3)$$

where :

$$\begin{aligned} A_\pm &= -(\gamma_1 \pm \gamma_2)(k_x^2 + k_y^2) - (\gamma_1 \mp 2\gamma_2)k_z^2 \\ B &= 2\sqrt{3}\,\gamma_3 [\ \{k_z , k_x\} - i\{k_y , k_z\}\ ] \\ C &= \sqrt{3}\ [\gamma_2(k_x^2 - k_y^2) - 2i\gamma_3\{k_x , k_y\}] \end{aligned} \qquad (3.4)$$

Here $\hat{I}$ is a unit 4x4 matrix and { , } denotes the anticommutator [4]. The calculation is done within the "axial model" in which [44] the parameters γ_2 and γ_3 in the C matrix elements of eqn.(3.4) are replaced by the mean value $\bar{\gamma} = (\gamma_2 + \gamma_3)/2$. [5]
($\gamma_1, \gamma_2, \gamma_3$ are the "true" Luttinger parameters that appear with a superscript L in APPENDIX F).
With this replacement, the Hamiltonian (3.3) acquires cylindrical symmetry about the z-axis and the resulting bands are isotropic in the k_x, k_y plane. For comparison, the true dispersions for $\vec{k}$ in the <100> and <110> directions are also shown in Fig.12 : the axial approximation represents a good average of them.
The labels on the vertical axis refer to the character of the solutions at $k_x = k_y = 0$, where there is no mixing of LH and HH components : the dispersion along k_z is purely parabolic, with effective masses

$$\begin{aligned} J_z &= \pm 3/2 \quad : \quad m_H^* = (\gamma_1 - 2\gamma_2)^{-1}\, m = 0.377\ m \\ J_z &= \pm 1/2 \quad : \quad m_L^* = (\gamma_1 + 2\gamma_2)^{-1}\, m = 0.091\ m \end{aligned} \qquad (3.5)$$

---

[4] We prefer to quote this more general form of the L.K. Hamiltonian written in terms of the anticommutators $\{k_x, k_y\}$ in view of its application when a magnetic field is present : in this case the different k-components do not in general commute.

[5] The axial approximation becomes necessary in the presence of a magnetic field applied along the z-direction : in such a case, as it will be explained in Paragraph 3.3, it is possible to write an exact solution for the motion in the (x,y)-plane only within the axial model.

As soon as one moves out of the $\vec{k}=0$ axis, the mixing of these components grows rapidly, leading to strong deviations from parabolicity. Notice in particular the first LH subband that starts off with a positive (i.e. electron-like) mass. The anti-crossing behavior leads in addition to a HH mass in the first subband heavier than expected in the absence of mixing.
The strong mixing at $\vec{k}\neq 0$ and the consequent non-parabolicity were first pointed out in Ref. [45]. For a symmetry-based justification of the anticrossing behavior in Superlattices, see Ref.[88] .

We will next see how these non-parabolicities lead to a complicate non-linear behavior of the Landau level structure when a magnetic field perpendicular to the interfaces is applied.

3.2. Oscillatory solutions inside the gap.

At this point, a word of caution must be said about the use of $\vec{k}\cdot\vec{p}$ matrices to describe the bulk band edges . The bulk Hamiltonian matrix (D.1) can have unphysical solutions: these spurious solutions are oscillatory in nature and correspond to values of the wave vector k that are outside the first Brillouin zone. They have their origin in the uncompleteness of the set of basis functions (2.16) used in the Kane approach, which makes it impossible to satisfy the periodicity relation $E(k)=E(k+2\pi n/a)$ in the BZ (a is the lattice constant, n=0,1,2...) [46] : one must be careful not to include these solutions in the construction of the superlattice wavefunction.

We have checked this point in our energy level calculation for bulk-GaAs by evaluating the expectation value $\overline{k_z}= < -d^2/dz^2 >$ for each particular level considered.
We found spurious, oscillatory ($\overline{k_z^2}>0$) solutions, with apparent Light hole character and with energy inside the energy gap, and such that $\overline{k_z} \simeq k_0= \pi/a = 0.55\ \mathring{A}^{-1}$ (a being the GaAs lattice constant). In the QW case, the acceptable solutions were characterized by a finite value of $\overline{k_z}$, much smaller than k_0, of the order of π/d as expected.

3.3. Removal of Kramers' degeneracy.

The Hamiltonian (D.1) is derived in the hypothesis that all the interacting bands have their double degeneracy (Kramers' degeneracy). In the absence of spin-orbit interaction this double degeneracy is associated with the electron spin that can be up or down without affecting the band structure.

Even in the presence of spin-orbit interaction this degeneracy remains, if the crystal has the diamond lattice [33]. On the other hand, the lack of inversion symmetry in zinc-blend materials like GaAs allows this degeneracy to be removed, through the appearance of additional terms, linear in the wave-vector k, in the off-diagonal elements corresponding to the four valence states in the matrix (D.1) [33].

All these terms are proportional to a constant C_K that has been recently measured for GaAs [47]. For example the splittings ΔE_H , ΔE_L for $\vec{k}$ along <110> direction between spin up and spin down hole states are given by :

$$\Delta E_H = (3\sqrt{3}/2)\ C_K k \quad , \quad \Delta E_L = (\sqrt{3}/2)\ C_K k \qquad (3.6)$$

The constant C_K is found to be $C_K(\mathrm{GaAs}) \cong -3.6$ meV·Å

Since at the wave vectors of interest in SL problems these splittings are extremely small, the linear k terms can be omitted in practical calculations.

A lifting of spin degeneracy, leading to a more sizeable spin-splitting of the valence subbands, results when there is a reflection-symmetry breaking due to asymmetric Superlattice potentials. This is the case of abrupt heterojunctions like the one of Fig.5 : the triangular potential well binding the holes clearly lacks inversion symmetry. The calculated spin-splitting of hole subbands in a GaAs/AlGaAs interface system can be as large as 5 meV at $k \sim 2 \times 10^6$ cm^{-1} (see Ref.[48]).

Another example concerns the "graded gap" heterostructures . Consider again the GaAs/$Al_xGa_{1-x}As$ system : if the compositional parameter x varies linearly across the supercell, one obtains the so-called "Sawtooth Superlattice", characterized by a spatial, approximately linear variation of the energy gap and the effective mass parameters (see, e.g., Ref. [49]). Valence subbands are spin-split due to the inversion asymmetry of this "sawtooth" superpotential : the splittings, which are very sensitive to the band-edge offset, vary between 4 and 7 meV at parallel momenta between π/d and $2\pi/d$ [50] .

CHAPTER IV

EXCITONS IN QUANTUM WELLS AND SUPERLATTICES

4. 3D and 2D Excitons

Excitons are bound electron-hole pairs and are the lowest electronic excited states in non-metallic crystals [52] .
In the case of a semiconductor with simple, isotropic valence and conduction bands with extrema at $\vec{k}=0$, and assuming a weak binding limit, the exciton spectrum is given by the solutions of an hydrogen-like Effective Mass equation and has the known form (see for example Ref. [53]) :

$$E_n = - Ry^* /n^2 \qquad (4.1)$$

(the zero of energy is taken at the bottom of the conduction band) Ry^* indicates an effective Rydberg

$$Ry^* \equiv e^4 \mu / 2\hbar^2 \varepsilon^2 \qquad (4.2)$$

Here μ is the reduced electron-hole mass, e the electron charge and ε the dielectric constant of the host material.
Excitons in optical spectra appear as sharp line structures just below the band gap, in contrast to the broad continuum transitions.

In QW structures, the exciton is modified because of the confinement of carriers in the potential well [6] .
If the layer thickness is smaller than the exciton Bohr radius, the exciton shrinks in one dimension: the electron and hole are forced to move closer to each other and the Coulomb binding energy increases. In the extreme case of a perfectly 2D exciton, this binding energy becomes [54] :

$$E_B^{(2D)} = 4\, Ry^* \qquad (4.3)$$

---

[6] In the following we restrict ourselves to the most relevant case in which both electrons and holes are confined within the same layer ,as it happens for example in the GaAs/AlGaAs systems.

This theoretical limit is never reached in real systems, due to finite barrier effect :it has been shown ([55] , [75]) that the binding energy in a Quantum Well first increases with decreasing layer thickness L_z and decreases in very narrow wells, the barrier height being kept constant.
The reason for this behavior is fairly simple : as L_z is reduced the exciton wavefunction is compressed in the QW, leading to increased binding . However, beyond a certain value of L_z, the spilling of the wavefunction in the adjacent AlGaAs layers becomes more important and this makes the binding energy go closer and closer to the bulk AlGaAs value.

In bulk GaAs one observes experimentally a single exciton resonance. The reduced symmetry of the QW structures, however, removes the light and heavy hole band degeneracy, and a two-exciton system results :in absorption experiments a double peak is observed.
Fig.13 reproduces early optical measurements on GaAs /GaAlAs QWs for three different values of the well width L_z (from Ref. [26]). The exciton peak shifts towards higher energies and splits into a LH and

Fig. 13

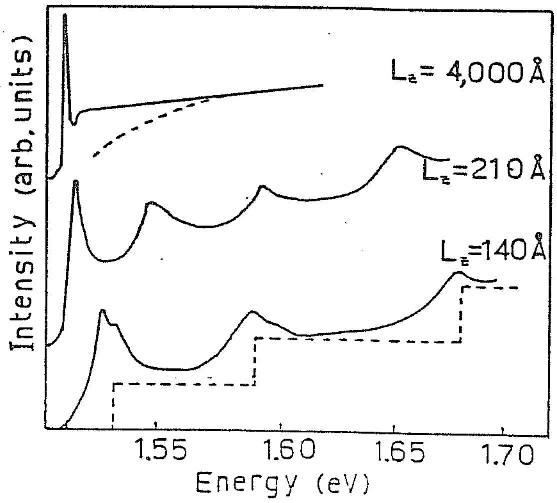

Absorption spectra at 2°K of 4,000 , 210 and 140 Å thick GaAs layers between $Al_{.2}Ga_{.8}As$ barriers (after Ref. 26). Dashed lines : schematic 3D (top figure) and 2D (bottom figure) Density Of States.

a HH component as the well becomes narrower and the system becomes two-dimensional (bottom figure).

Note also the different structure of the background spectrum due to transitions to the continuum ,which reflects directly the different dimensionality of the systems : the dashed lines show ,respectively in the top and bottom figure, the schematic Density Of States for 3D (proportional to $\sqrt{E}$) and for 2D systems, for simple parabolic bands: in the 2D case, each of the two-dimensional subbands gives rise to a DOS that is independent of the energy and equal to $m^*/\pi\hbar$, so that the cumulative DOS for a series of bands will have the staircase-like form shown.

4.1. Excitons in cubic semiconductors

For realistic calculations of the exciton spectrum in cubic semiconductors, the valence band degeneracy near $\vec{k}=0$ must be taken explicitly into account.

The bulk effective mass Hamiltonian for excitons can be written as :

$$H_{exc} = H_e(\vec{p}_e) - H_h(\vec{p}_h) - e^2/\varepsilon r \qquad (4.4)$$

Here the first term is simply $p_e^2/2m_e^*$, the second is the 4x4 Luttinger Hamiltonian (3.3) for the holes,$\vec{r}$ is the relative coordinate $\vec{r} = \vec{r}_e - \vec{r}_h$. (The electron term and the Coulomb term are assumed to be multiplied by a unit 4x4 matrix); the overall momentum of the pair $\vec{P} = \vec{p}_e + \vec{p}_h$ is actually a constant of the motion and has been taken to be zero.

The simplest approximation that can be done on the Hamiltonian (4.4) consists in the neglecting of the off-diagonal elements ,that are proportional to γ_2 and γ_3 , and in retaining only the diagonal ones, that are proportional to $\gamma_1 + 1/m_e^*$ For GaAs, $m_e^* = 0.067$, $\gamma_1=6.85$, $\gamma_2=2.1$, $\gamma_3=2.9$: therefore $\gamma_1 + 1/m_e^* \gg \gamma_2, \gamma_3$. Thus one finds four degenerate exciton states with energy given again by the effective Rydberg Ry (4.2), with a reduced mass given by $\mu^{-1} = \gamma_1 + 1/m_e^*$. In particular , $Ry^*_{GaAs}=3.9$ meV (using the value ε =12.57) ,while the experimental binding energy is $\sim$4.2 meV [26].The corresponding effective Bohr radius is $a_0^* = \hbar^2\varepsilon/\mu e^2 \sim 145$ Å, showing that the ground state hydrogenic wavefunction is widely spread over the lattice; this result justifies a posteriori, the use of the EM approximation for this system. The off-diagonal terms of H_h can eventually be included as a second-order perturbation.

In a QW, this procedure cannot be carried out for two reasons : (i) the absence of translational invariance in the z-direction makes P_z (the z-component of the total momentum of the pair) to be no longer a good quantum number; (ii) the boundary conditions depend separately on the coordinate z_e , z_h and not on $z_e - z_h$ only.
This makes the exciton problem in QW structures much more complicated than for the bulk: in fact, a detailed calculation of the exciton binding energy in a QW has not yet been performed.
A commonly used simplification (see for example Ref. [56]) considers two uncoupled HH and LH bands, with effective masses :

$$1/m_H^* = \begin{cases} \gamma_1 - 2\gamma_2 & \text{in the z-direction} \\ \gamma_1 + \gamma_2 & \text{in the x,y direction} \end{cases} \qquad (4.5)$$

$$1/m_L^* = \begin{cases} \gamma_1 + 2\gamma_2 & \text{in the z-direction} \\ \gamma_1 - \gamma_2 & \text{in the x,y direction} \end{cases} \qquad (4.6)$$

Then two sets of excitons result, whose binding energies are obtained by a variational trial wavefunction ,usually chosen of the form :

$$\Psi_{ex}(\vec{r}) = f_e(z_e) f_h(z_h) g(x,y,z) \qquad (4.7)$$

x,y,z being the relative coordinates :$f_e(z)$ and $f_h(z)$ represent the exact solutions for the finite square well problem, while g (x,y,z) describes the internal motion of the exciton.
One decisive drawback of this approach is that it gives, in the limit $L_z \longrightarrow \infty$,two excitons instead of a four-fold degenerate ground exciton state appropriate to a bulk situation;similarly,as $L_z \longrightarrow 0$, one gets still two split excitons for the (bulk) materials making up the walls.

A more realistic approach should include, at the very beginning, the admixture between LH and HH subbands, in order to get the correct asymptotic behavior.

4.2. Two-dimensional hydrogenic exciton in a uniform magnetic field.

Consider the following Effective Mass equation describing the relative motion of an electron - hole pair in the presence of an external magnetic field parallel to the z-axis [53] :

$$[(\vec{p} -(e/2c)\vec{B}\wedge\vec{r})^2/2m_e^* + (\vec{p} +(e/2c)\vec{B}\wedge\vec{r})^2/2m_h^* - e^2/\varepsilon r]\,\Phi(\vec{r}) = E\,\Phi(\vec{r}) \qquad (4.8)$$

Here ε is the dielectric constant of the host material.
It is a common practice to introduce a dimensionless parameter γ to indicate the relative strengths of the magnetic field effect and Coulomb interaction :

$$\gamma \equiv \hbar\omega_c/2Ry^* \qquad (4.9)$$

Here $\hbar\omega_c = e\hbar B/\mu c$ is the cyclotron effective energy, μ being the reduced electron-hole mass.
Many attempts have been made to solve eqn.(4.8) by perturbation theory ($\gamma \ll 1$), by the adiabatic approximation ($\gamma \gg 1$) and by variational methods (Ref.[53] and references therein).

Let's consider the case of a hypothetical Two-Dimensional hydrogenic exciton in a uniform magnetic field : this problem is somewhat related to the problem of excitons in Quantum Wells, due to the quasi-2D behavior induced by quantum confinement.
For this 2D case the problem reduces to solve the following differential equation [57] :

$$-\hbar^2/2\mu[1/r\, d/dr(r d/dr)+m^2/r^2]R(r)+(-e^2/\varepsilon r + e^2B^2r^2/8\,c^2\mu)R(r)=E'\,R \qquad (4.10)$$

Here m is a magnetic (integer) quantum number and the energy E' is related to E as follows :

$$E' = E - [(m_e^* - m_h^* / m_e^* + m_h^*) eB/2\mu c] m \qquad (4.11)$$

We will consider only the case m=0 . This corresponds to the "allowed case" of the optical excitation spectrum, which is the most important from the experimental point of view [53] .
We will quote only some limiting expressions of the eigenvalue spectrum of eqn. (4.10), obtained in a WKB approximation, that will be used later in connection with the problem of interpreting the experimental data of magneto-absorption in Quantum Wells. For a discussion of equation (4.10) and its solutions, see Ref.[57] .

(a) For vanishing magnetic field (*exciton* case) one has :

$$E = -[1/(n+1/2)^2] \mu e^4 / 2\hbar^2 \varepsilon^2 \ , \ n=0,1,2,... \qquad (4.12)$$

(b) For vanishing Coulomb interaction (*Landau level* case) :

$$E = (n+1/2)\, \hbar eB/\mu c = 2\gamma(n+1/2) \qquad (4.13)$$

(c) In the *weak* magnetic field region ($\gamma \ll 1$) :

$$E = -1/(n+1/2)^2 + 5/8(n+1/2)^4 \gamma^2 \qquad (4.14)$$

(d) In the *strong* magnetic field region ($\gamma \gg 1$) :

$$E = (2n+1)\gamma - 3\{\gamma/(2n+1)\}^{1/2} \qquad (4.15)$$

The last type of square root dependence can be obtained by treating the Coulomb term $e^2/\varepsilon r$ as a perturbation acting on the free-particle states $|n\rangle$ that are solutions of the 2D harmonic-oscillator equation to which eqn.(4.10) reduces when the Coulomb interaction is absent. Thus the first order correction to the unperturbed Landau level spectrum is given by :

$$\langle n| e^2/r |n\rangle \cong e^2/a_n = (m\omega/\hbar) e^2/(2n+1)^{1/2} \qquad (4.16)$$

where a_n is the mean orbit radius for a 2D oscillator of frequency : thus excitonic effects are expected to be less important for large quantum number n .
In the high field limit $\gamma \longrightarrow \infty$, the second term in (4.15) can be neglected and one recovers the Landau level free-particle behavior.

We reported in Fig.14.a the calculated level, solutions of eqn.(4.10), for field strengths up to γ =1. (from Ref. [57]). The lowest level (n=0) looks independent of the magnetic field up to γ~1, but in higher magnetic field region it goes parallel to the corresponding free Landau level, after crossing the E=0 line at $\gamma \cong$ 12.5 .

In Fig. (14.b) are reported also the calculated relative intensities for optical excitations in the states m=0, which are proportional to the squared modulus $|R(r=0)|^2$, as a function of the quantum number n for several values of the reduced field . The relative intensity for the n=0 transition, not shown in the figure, is roughly independent of γ and equal to ~ 16 ,in the same units used in the figure. Apart from the n=0 case, the intensities are essentially independent of the quantum number n.

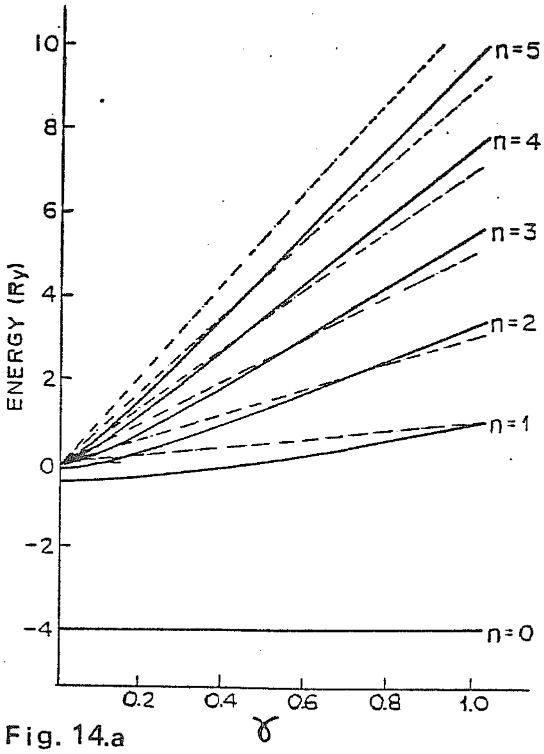

Fig. 14.a

Energy eigenvalues as functions of the magnetic field strength γ. The broken lines denote the free Landau levels.

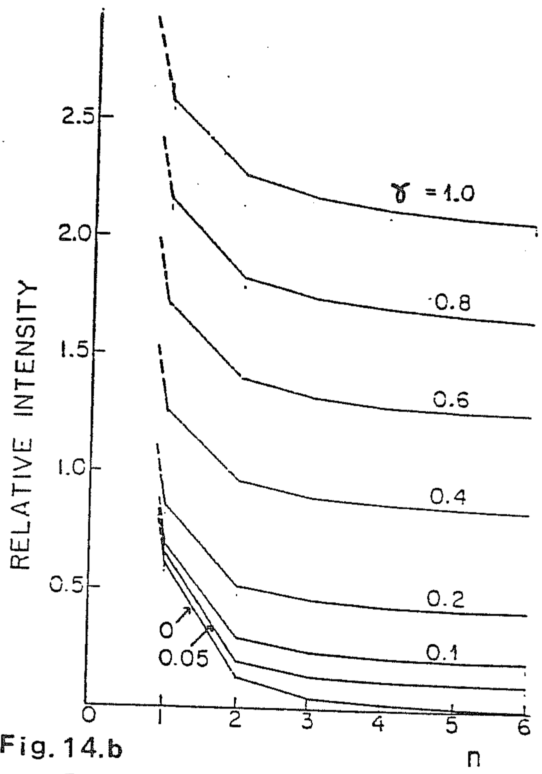

Fig. 14.b

Relative intensities vs. the quantum number *n* for several fixed values of γ

Expressions (4.12) to (4.15) form the basis of a simple interpretation scheme of excitonic effects in magneto-absorption experiments in QW's that will be used in the following Chapter.

4.3. Excitonic effect in Magneto-absorption experiments

The structure of the magneto-optical spectra in GaAs QW has been interpreted by several authors ([58] , [59]) in terms of transitions between free-carrier Landau levels, of which only the lowest n=0 is affected by appreciable excitonic effects. This is known, however, not to be the case in bulk GaAs in which Coulomb binding is significant at high fields even in the higher levels : the inclusion of excitonic effect is necessary in order to correctly interpret the observed spectra [60] .

The evident non-linear behavior of the peak positions on magnetic field ,in contrast with the prediction of the Landau level theory, has been clearly shown for the first time by the magnetic absorption experiments on Ge [61] .
In their pioneering work, Elliott and Loudon ([62] , [63]) considered the effect of the Coulomb interaction between electrons and holes in a simple parabolic band picture : their conclusion was that there is an exciton series associated with each Landau level and that the most important absorption peaks in the magneto-absorption spectra correspond to the transitions to these exciton levels.

The problem of complex-band excitons in a magnetic field is much more complicated (see, for example, Ref. [64]),although approximate methods has been developed for the two limiting cases of high and low magnetic fields when either the Coulomb interaction or the magnetic field can be treated as a perturbation.

In type-I Quantum Wells, due to the higher binding energy of excitons, the effect of the Coulomb interaction is expected to play a major role in the interpretation of magneto-optical spectra, even at high magnetic fields.
We will take into account excitonic effects in our calculation of inter-Landau level transitions within a simple scheme (used also in

Ref. [65]) , which follows the treatment of excitons in magnetic field in highly anisotropic system given in Ref. [57].
We already gave a brief account of this theory in the previous Paragraph.

CHAPTER V

LANDAU LEVEL CALCULATION AND COMPARISON WITH MAGNETO-OPTICAL EXPERIME

5. Landau Level calculation

The energy levels are obtained by solving the following set of coupled EM equations [7] :

$$\sum_j H_{ij} F_j = E F_i \qquad (5.1)$$

where H_{ij} is the Hamiltonian (2.30) and F_j is the j-th component of the vector (2.29). The total zeroth-order wavefunction is given by

$$\Psi = \exp(ik_{sz} z) \sum_j F_j u_j \qquad (5.2)$$

and k_{sz} is the quasi-momentum in the SL-Brillouin zone.

We have applied to eqn.(5.1) the method of solution described in Chapter II, to obtain the Landau Levels (LL) for electrons and holes in a QW geometry (i.e. we put $k_{sz}=0$ in the expression (5.2) for the wavefunction). The band parameters used in the calculation are listed in APPENDIX F.

From the non-parabolic behavior of the hole subband dispersion with the in-plane wave vector k shown in Fig.12, one can predict a strong non-linear dependence of the hole energies versus the magnetic field strength B : for high oscillator quantum number n this can be seen from the semi-classical limit, according to which the Landau levels of a subband E(k) are given by the correspondence

$$E\,(B) = E(\,k=\sqrt{2eBn/c}\,), \qquad \text{for } n>>1$$

---

[7] We shall consider systems made of intrinsic semiconductors, for which no charge accumulation in the Quantum Well is expected : in this case the potential term $U(\hat{r})$ in eqn.(2.18) is zero, corresponding to wells with flat bottom.

The calculated hole and electron Landau levels for the case of a 78 Å-QW between $Al_xGa_{1-x}As$ barriers ($x=0.3$) are shown in Fig.15 and Fig.16 . They are obtained using a 60/40 % rule for the band-offset (see Section 5.3.1 for a related discussion).

Before comparing the theoretical results with magneto-absorption experimental data, it is useful to underline some interesting characteristics of these level structures.
The most remarkable feature of the calculated hole Landau levels is represented by their strong non-linear behavior. This non-linearity comes from the fact that the HH and LH subbands are decoupled only at $\vec{k}=0$ (or, equvalently, at $B=0$). At $B\neq0$ Landau levels originating from the first HH subband interact with LL from the next LH subbands and give rise to the anticrossing behavior shown in the figure, with a consequent flattening of the dispersion relation of the HH subbands. In general, this Landau level structure can no longer be described in terms of one effective mass per subband.

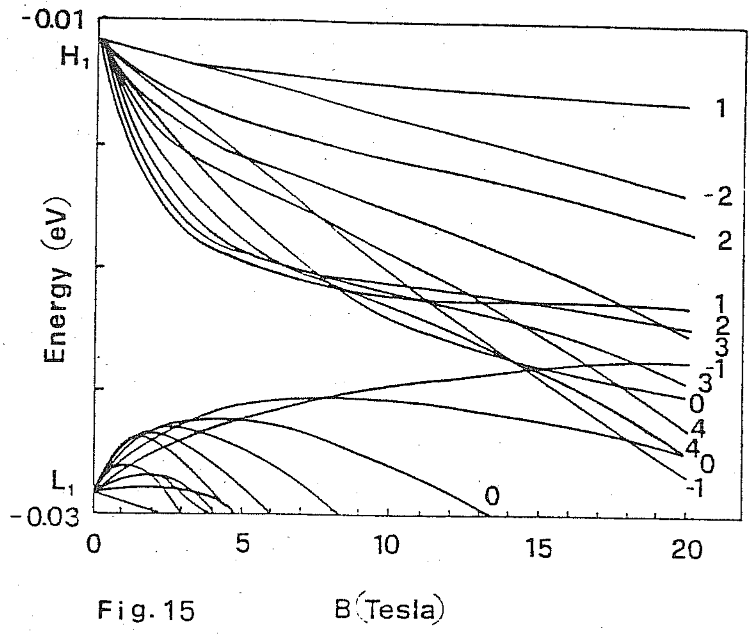

Fig. 15

Calculated Landau levels for two hole subbands in a 78 Å $GaAs/Al_{.3}Ga_{.7}As$ Quantum well.
The numbers are the Landau level indices.

Fig.16

Calculated Landau levels for two electron subbands in a 78 Å GaAs Quantum Well.
The numbers are the Landau indices n.

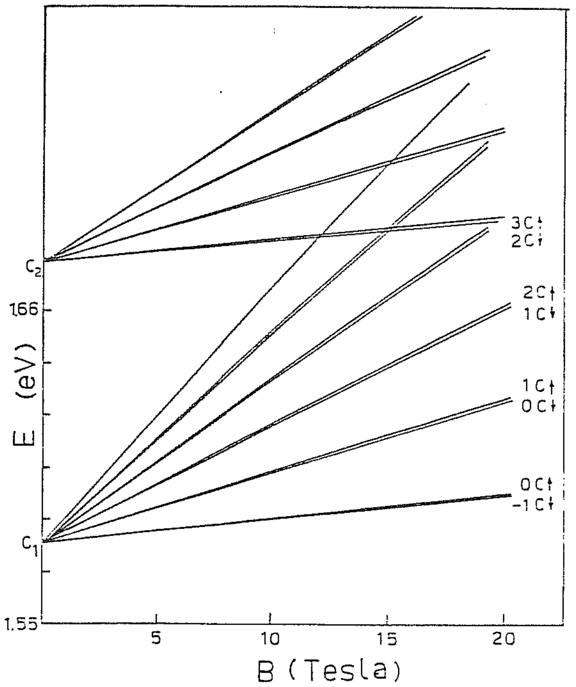

The electron levels shown in Fig.16 are much more regular, displaying a simple "Landau ladder" form . Their energy (measured from the conduction subband edge C_1 at B=0) can be roughly approximated by the "free-particle" expression:

$$E_n = \hbar\,\omega_c^*(n+1/2) \pm (1/2)\mu_B|g^*|\,B \qquad , n=0,1,2\ldots \qquad (5.3)$$

Here $\hbar\omega_c^* = \hbar eB/m^*c$ is the cyclotron energy, μ_o is the Bohr magneton , g^* the effective g-factor of the electron and n is the Landau level index. The appropriate effective mass is given, in a three band model (see section 5.1) by the following expression [66] (atomic units are used) :

$$1/m^* = 1/m + (2P^2/3)\,[\,2/E_g + 1/(E_g+\Delta)\,] \qquad (5.4)$$

The g-factor is given, within the same model, by the expression :

$$g^*/2 = 1 - 2P^2/3[\,1/E_g - 1/(E_g+\Delta)\,] \qquad (5.4b)$$

We note that the spin-splitting term in eqn.(5.3) :

$$H_s = \pm(1/2)\mu_B|g^*|B \qquad (5.5)$$

is very small, due to the smallness of g^*($g^*(GaAs) = -0.44$) : at 20 Tesla, $|H_s| \simeq 0.5$ meV.

At high fields the electron Landau levels display slight deviations from a linear behavior, especially for large n : in particular, the separation between successive levels, at a fixed value of B, decreases with increasing n.
These effects must be ascribed to non-parabolicity in the conduction band due to the coupling with valence band states.

5.1. Non-parabolicity

The mixing between conduction and valence band states via the P matrix element (2.14) leads to non-parabolicity in the conduction band. In a quantizing magnetic field B, within a three band Kane model that treats perturbatively the coupling between the conduction Γ_6 and the valence Γ_7^v and Γ_8^v edges and neglect the small spin-splitting terms, the explicit expression of the Landau levels band edge is given by [67] :

$$E'_n = \hbar\omega_c^*(n+1/2)\{\ 1+\frac{K_2}{E_g}\hbar\omega_c^*(n+1/2)\ \} \qquad (5.6)$$

where the constant K_2 is given by :

$$K_2 = -\frac{(1-m^*/m)^2 E_g(3E_g+4\Delta+2\Delta^2/E_g)}{(E_g+\Delta)(3E_g+2\Delta)} \qquad (5.7)$$

Here m^* is the effective band-edge mass as given by eqn.(5.4)
For GaAs, K_2= -0.83, assuming an effective mass m^* =0.0665m [68].
The first term in eqn.(5.6) describes the undisturbed LL corresponding to a parabolic band and the second represents a small non-parabolic correction which depends quadratically on B.

A more accurate description of non-parabolicity should include in principle the coupling with higher bands [69] (typically the Γ_7^c and Γ_8^c conduction band minima in GaAs, see fig.17) : however, the matrix elements of these interactions are not known precisely enough and the size of the problem becomes bigger.
For example, a 8x8 Kane model, which treats directly the $\vec{k}\cdot\vec{p}$ coupling between the Γ_6^c conduction band and the $(\Gamma_7^v+\Gamma_8^v)$ valence band edges, and by perturbation theory the coupling to higher $(\Gamma_7^c+\Gamma_8^c)$

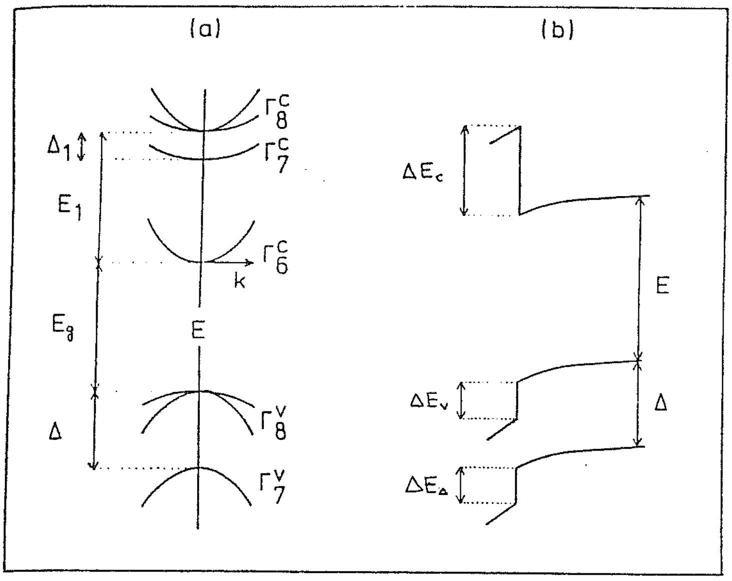

Fig. 17 (a) Energy band structure at the Γ point in five-level approximation. (b) Band edges in a heterostructure with abrupt interface (the higher conduction band is not indicated).

conduction bands, is found to describe quite accurately the non-parabolicity up to energies 50 meV above the Γ_6^c conduction band minimum [70].

For higher energies, a 14x14 matrix is required, which considers the coupling to the second conduction band edges in an exact way.

In particular the 8x8 model systematically underestimate the effective mass : In the (110) direction, for example, the effective masses given by the two models differ by approximately the 16% at 150 meV [70].

In a QW, the conduction band can be described again by an expression of the form (5.6), but in which the term $\hbar\omega_c^*(n+1/2)$ is replaced by $\hbar\omega_c^*(n+1/2) + \hbar^2 k_z^2/2m^*$. The terms in k_z^2 arise from the quantum confinement and make the non-parabolic corrections more important in heterostructures than in bulk semiconductors.

For a thorough discussion of the $\vec{k}\cdot\vec{p}$ description of conduction band electrons in heterostructures, see Ref. [66]

5.2. Interband optical transitions : selection rules and transition amplitudes

Let's consider the process in which a photon is absorbed and an electron is raised from a valence band-Landau level to a conduction band one.

The total zeroth-order wavefunction in each material is given by the expression (see (5.2) and (2.29)) :

$$\Psi_n = \sum_{1}^{6}{}_j \; u_j \; F_j^n \qquad , \; n=-2,-1,0,\ldots \qquad (5.8)$$

where F_j^n is the j-th component of the vector (2.29) :

$$F_n=(c_1(z)\varphi\, n, c_2(z)\varphi\, n-1, c_3(z)\varphi\, n+1, c_4(z)\varphi\, n+1, c_5(z)\varphi\, n, c_6(z)\varphi\;\, n+2)$$
(5.9)

,u_j being members of the basis set (2.16) and φ_n harmonic oscillator functions. The $c_j(z)$ envelope-functions must be set to zero for those components that have a negative oscillator index n : for example, when n=-2, only the 6-th component $c_6(z)$ (corresponding to the $|3/2;-3/2\rangle$ HH state) is present in the expansion (5.8).
Indicating with I and F, respectively, the initial (valence) and final (conduction) states with Landau index n,n' respectively, the matrix element for direct optical transitions is given by

$$M_{nn'}= \langle \Psi_n^I | \vec{p}\cdot\vec{\varepsilon}\, | \Psi_{n'}^F \rangle = \sum_{jj'} \langle u_j | \vec{p}\cdot\vec{\varepsilon}\, | u_{j'} \rangle \langle F_j^n | F_{j'}^{n'} \rangle + \sum_{jj'} \vec{\varepsilon}\cdot \langle F_j^n | \vec{p} | F_{j'}^{n'} \rangle\, \delta_{jj'} \quad (5.10)$$

Here we use the compact notation :

$$\langle u_i | u_j \rangle \equiv \int_{cell} u_i^*(\vec{r}) \; u_j(\vec{r}) \; d\vec{r}$$

$$\langle F_i | F_j \rangle \equiv \int_{crystal} F_i^*(\vec{r}) \; F_j(\vec{r}) \; d\vec{r}$$

The indices j,j' run over the set of six envelope functions and the Kronecker' delta $\delta_{jj'}$ comes from the orthogonality of Bloch functions with different symmetry. Here $\vec{\varepsilon}$ is a unit vector in the direction of the electric field of the incident radiation [8]

---

[8] In these experiments both the incident and emitted radiation propagate at right angles to the layer plane and parallel to the magnetic field axis (Faraday configuration) : the exciting light is either left (σ^+) or right (σ^-) circularly polarized with respect

The first term on the right hand side gives the allowed transitions at $\vec{k}=0$ [71]. The second term, which is small compared with the first term, gives the forbidden transitions at $\vec{k}=0$ .These latter arise in zinc-blend materials because of the lack of inversion symmetry. We will consider only the first term in (5.10).

The intensity of an inter-Landau level transition $n \longrightarrow n'$ between state I and state F is thus proportional to the squared dipole matrix element :

$$|M_{nn'}|^2 = |\langle \Psi_n^I | \vec{p}\cdot\vec{\varepsilon} | \Psi_{n'}^F \rangle|^2 = \left| \sum_{jj'} \langle u_j | \vec{p}\cdot\vec{\varepsilon} | u_{j'} \rangle \int c_j^*(z)\, c_{j'}(z)\, dz \int \varphi_{m_j}^* \varphi_{m_{j'}} d\vec{r} \right|^2$$

$$= \left| \sum_{jj'} (\vec{p}\cdot\vec{\varepsilon})_{jj'} \int c_j^*(z)\, c_{j'}(z) dz\ \delta_{m_j, m_{j'}} \right|^2$$

(5.11)

where $m_j, m_{j'}$ are the j-th and j'-th component of the vector

$$M = (n, n-1, n+1, n+1, n, n+2) \qquad (5.12)$$

Since the only matrix elements $(\vec{p}\cdot\vec{\varepsilon})_{jj'}$ different from zero ,in circularly polarized light, are :

$$|(\vec{p}\cdot\vec{\varepsilon})_{12}|^2 = P^2/2 = |(\vec{p}\cdot\vec{\varepsilon})_{46}|^2 = (1/3)\,|(\vec{p}\cdot\vec{\varepsilon})_{13}|^2$$
$$|(\vec{p}\cdot\vec{\varepsilon})_{45}|^2 = |(\vec{p}\cdot\vec{\varepsilon})_{13}|^2 \qquad (5.13)$$

P being the Kane matrix element (2.14), one sees by inspection that the selection rule

$$\Delta n = \pm 1 \qquad (5.14)$$

must be satisfied .

In addition to the selection rule for n, the change in the total angular momentum must be $\Delta M_J = \pm 1$, in the Faraday configuration, respectively for σ^+ and σ^- radiation : thus the plus sign in (5.14) holds for one circular polarization of light, the minus sign for the other.

---

to the magnetic field direction.

We summarize in the following table how the various components of the wavefunction (5.1) are involved in the transitions, for the two different polarizations. We make use of the shorthand notation with "up" and "down" spin for electrons and holes, as indicated on the left of the figure, together with the angular momentum quantum numbers for each state.

The oscillator strength of an H component is 3 time bigger than the L one, as a consequence of the paticular form of the atomic-like dipoles $(\vec{p}\cdot\vec{\varepsilon})_{ij}$ (5.13) associated with the basis set (2.16): we thus expect that the transitions from H hole Landau levels be more intense than those involving L hole levels.

This is represented by the thicker lines connecting the states involved.

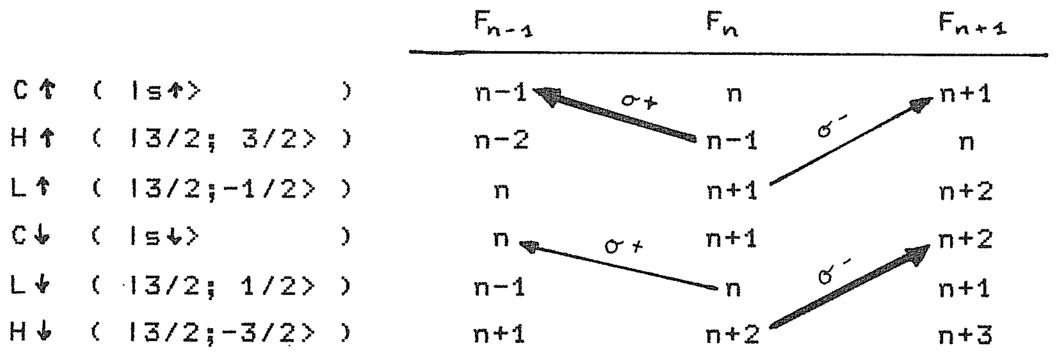

		F_{n-1}	F_n	F_{n+1}
C↑	($\vert s\uparrow\rangle$)	n−1	n	n+1
H↑	($\vert 3/2;\ 3/2\rangle$)	n−2	n−1	n
L↑	($\vert 3/2;-1/2\rangle$)	n	n+1	n+2
C↓	($\vert s\downarrow\rangle$)	n	n+1	n+2
L↓	($\vert 3/2;\ 1/2\rangle$)	n−1	n	n+1
H↓	($\vert 3/2;-3/2\rangle$)	n+1	n+2	n+3

(5.15)

We stress the fact that in a simple scheme that uses only the selection rule (5.14) to determine the allowed transitions between Landau levels, far more transitions are predicted than experimentally observed [58], whereas the mixing between L and H hole subbands, together with the restrictions imposed by (5.15), makes many of the allowed transitions have a vanishing matrix element : the resulting picture of magneto-optical transitions is neither simple nor obvious.

In addition, transitions that are allowed by the selection rules stated above can have vanishing matrix elements due to the different parity of the envelope-functions $c_j(z)$ of the initial and final state (see the next Paragraph).

Thus the explicit evaluation of the matrix elements (5.11) seems to be a fundamental ingredient in any attempt to make a detailed and quantitative comparison between theory and experiment. Before making this comparison, we will discuss briefly in the following section the essential symmetry properties of the envelope functions $c_j(z)$ appearing in the overlap integrals in (5.11).

5.2.1. Symmetry properties of the Envelope-Functions

The SL potentials that enter into the diagonal terms of the Effective Hamiltonian governing the envelope functions, are even with respect to the centers of both the well and the barrier layers [9] if flat-band conditions prevail, as it is usually assumed in the case of undoped heterostructures, the SL potential is simply given by the discontinuities ΔE_c, ΔE_v in the band edges when going from one material (A) to the other (B) and has the square-wave profile of Fig.2 .

In the expansion (5.8) each envelope function $c_j(z)$, $j=1,..,6$, is a solution of a 1x1 effective Hamiltonian H ,obtained by projecting the 6x6 effective Hamiltonian onto the j-th edge.

It can be shown [72] that H contains only even powers of $\partial/\partial z$ [10] thus every $c_j(z)$ can be either even or odd with respect to the reflections in one of the mirror (x,y)-planes bisecting the A and B layers .

In particular at B=0, when there is no mixing between hole states ,the usual optical selection rule

$$m' - m = \text{even integer} \qquad (5.16)$$

is expected to hold, m' and m being the subband indices of the valence (H or L) and conduction (C) states involved [11]

---

[9] This is strictly true if any inversion-asymmetry effect associated with the zinc-blend lattice is neglected ("Quasi-Ge" model).

[10] We recall that, in the EM approach, the z-component of the wave vector k has to be replaced by the operator $k_z = -i\hbar\partial/\partial z$ which operates on the envelope functions $c_j(z)$.

[11] It is implicitly assumed that the C-states are essentially decoupled from the hole states : we found that the hole components in Landau levels originating from the C subband, with $n < 7$, are always less than 5 % of the norm of the eigenvector.

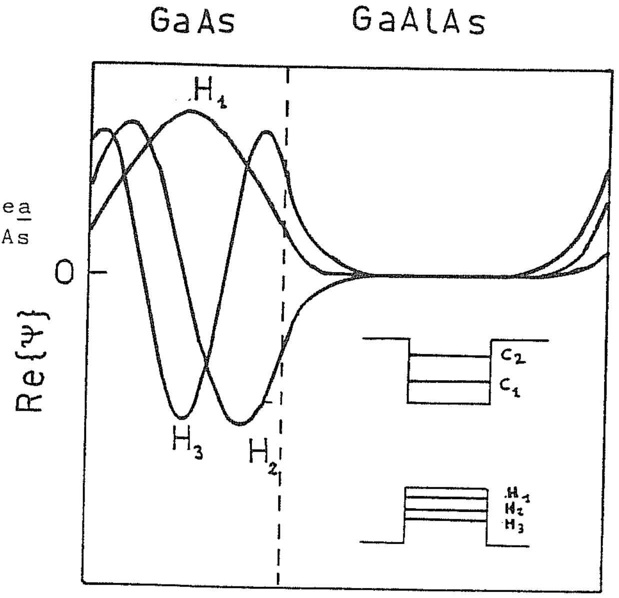

Fig. 18

Wavefunctions associated with the highest three Heavy hole subbands in a GaAs Quantum Well at B=0 .

In Fig.18 we report the zero-field Heavy hole wavefunctions H_1, H_2, H_3 for the highest three subbands in a 78 Å GaAs QW : the even and odd characters are evident ;the conduction subbands C_i,not shown, exhibit analogous symmetries. The zero-field $H_2 \longrightarrow C_1$ transition is thus parity forbidden, whereas the $H_3 \longrightarrow C_1$ one is expected to be present but with minor strength than the principal $H_1 \longrightarrow C_1$. The same is true for L-C transitions.

Consider now the bulk Hamiltonian (E.1). For $B \neq 0$, the H↑ state is coupled with the L↓ state by a term proportional to k_z and to H↓ by a term independent of k_z. Because k_z is odd under the reflection with respect to the mirror planes (see Footnote [9]), an even H↑component will be coupled with an odd L↓and an even H↓and vice versa. A similar argument applies to the coupling between H↓,L↑ and L↓ states.

To illustrate this point, we show in Fig.19 the squared amplitudes $|c_j(z)|^2$ for each of the hole components (j=2,3,5,6) of the envelope function (5.8) for the 78 Å GaAs Quantum Well between $Al_xGa_{1-x}As$ barriers, calculated at B=10 Tesla, plotted as a function of the SL coordinate z (for the notation, see the first column in Table 5.15) : the four figures refer to the highest (in energy) four hole-Landau levels with n=1. The arrow indicates where the interface between GaAs and AlGaAs is located.

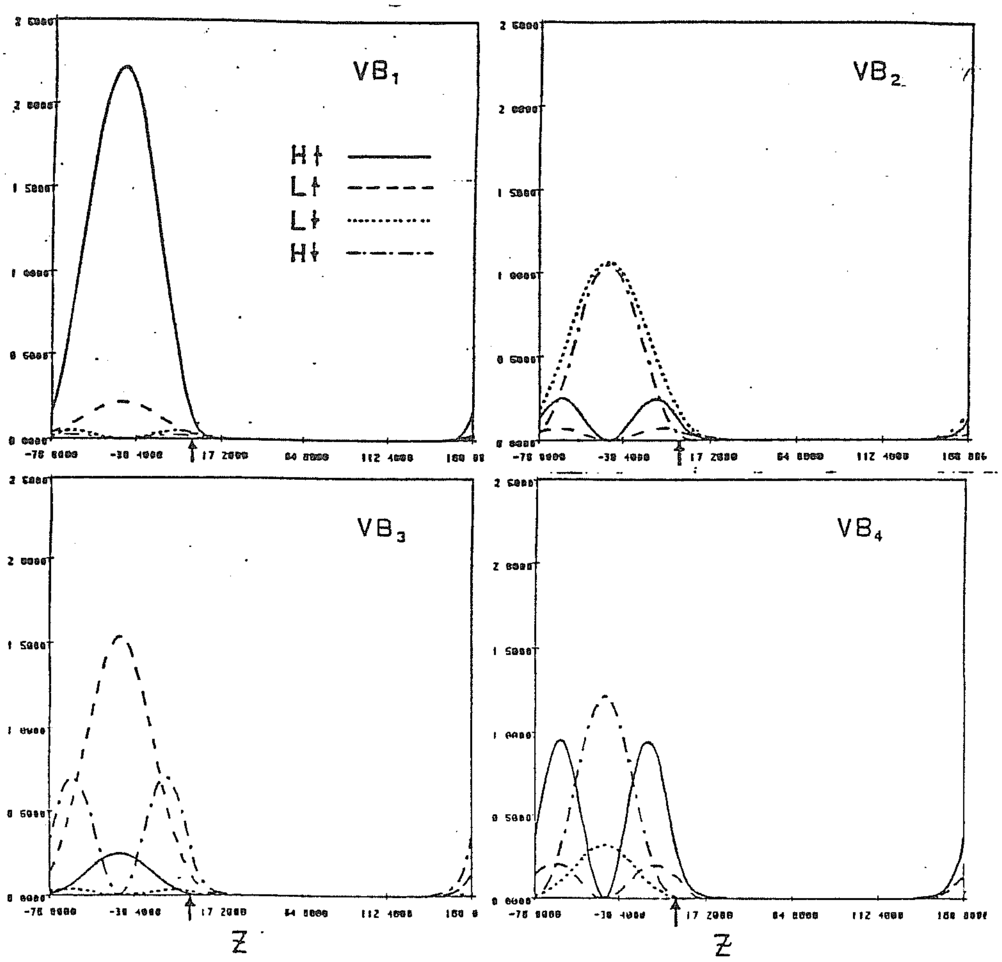

Fig. 19

Squared amplitudes associated with the four components (indicated in the first panel)of the envelope-functions for the four highest valence states with Landau index n=1, at B=10 Tesla.
The arrow indicates where the interface is.

The strong admixture between the H and L components is clearly visible in the VB2,VB3,VB4 states : only the highest VB1 state displays a dominant H↑ character. As anticipated, H↑ [H↓] and L↓[L↑] states are mixed with opposite parity. The total wavefunction, not shown, doesn't exhibit any particular reflection symmetry.

We stress the fact that this mixing is peculiar to QW systems, since the k_z coupling comes in as a consequence of quantum confinement : the approximation k_z =0 [73] that is commonly used in the analysis of magneto-absorption in bulk materials when the magnetic field is along the z-direction, is meaningless in this context.

We will exploit the above mentioned symmetry properties of the envelope- functions in our analysis of magneto-absorption experiments in Quantum Wells.

5.3. Comparison with Magneto-Optical experiments.

We made a comparison with the results of excitation spectroscopy experiments performed in a 78 Å GaAs Quantum Well cladded between thick AlGaAs layers, at high field (up to 20 Tesla) and at very low temperature, in the Faraday configuration (see Footnote at page 49).

In Fig.20 is shown the excitation spectrum at B=0 : the two exciton peaks associated with the first H_1C_1 and L_1C_1 transitions are clearly visible ; the two shallow bumps superimposed on the constant background (which reflects a quasi-2D density of states) are attributed to higher exciton levels, namely H_3C_1 and H_2C_2.
At $B\neq0$ several peaks are observed, corresponding to direct interband transitions between valence and conduction bands, as the continuum

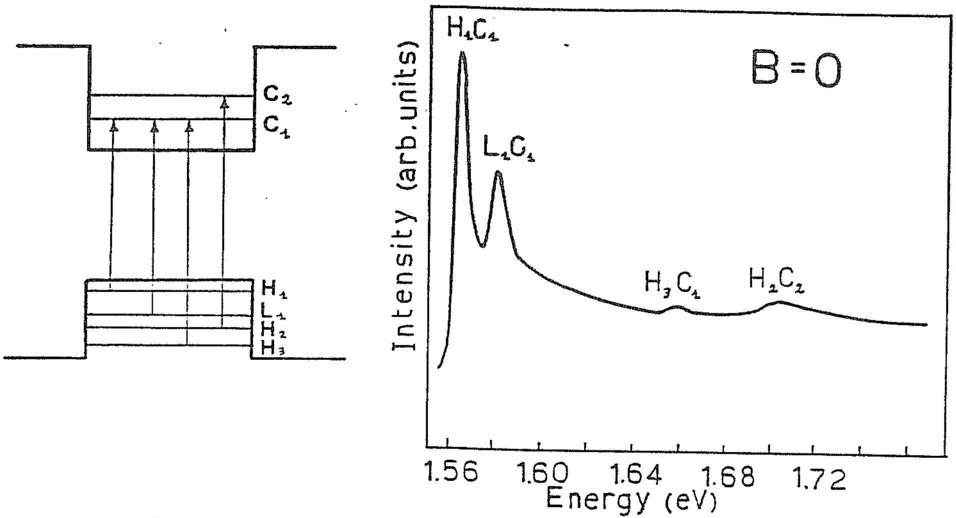

Fig. 20

Excitation spectrum at B=0.
On the left part of the Figure the transitions associated with the observed exciton peaks are shown.

states split into Landau levels.

5.3.1. Band-offset determination.

An important input parameter in the calculation is the band-offset Q_c . (see Paragraph 1.4).
We have estimated this quantity, following Ref. [74] ,by fitting the energy of the observed peaks at B=0 : we attributed the two sharp peaks and the two shallow ones in Fig.20 to excitonic transitions between the conduction C and the Light or Heavy holes (L, H) subband edges, as shown in the left part of the figure. The calculated dependence of the corresponding transition energies upon the conduction band discontinuity Q_c is also shown in the diagram in Fig.21 : note the strong dependence of the H_3C_1 transition energy on Q_c. The arrows drawn on the left side indicate the experimental observed values,obtained directly from Fig.20, and corrected for the binding energies of the excitons :we used for these latter quantities the theoretical values quoted in Ref. [75] , obtained with a variational method (they range from ≃6 meV for the binding energy of the H_2C_2 exciton to ≃10 meV for the L_1C_1).

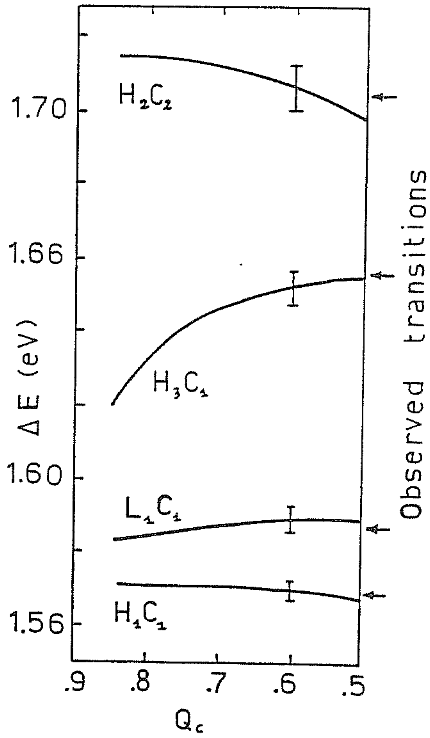

Fig. 21

Calculated dependence of the transition energies at B=0 on the conduction-band discontinuity $Q_c = \Delta E_c / \Delta E_g$.
The observed transitions,corrected for the binding energies of the excitons as explained in the text, are indicated by arrows.
The bars drawn at Q_c=0.6 account for a possible uncertainty of ± 2Å in the well width.

We found that the best fit to experimental data is obtained assuming $Q_c \cong 0.6$ .Our estimate is in rough agreement with the most recent determinations of Q_c as reported in Paragraph 1.4 . [28]
The bars drawn on the curves at this value, account for a possible uncertainty of ± 2 Å on the GaAs well thickness.

5.3.2. Calculated interband transition energies and strengths

In Fig.22 we show the calculated interband transition energies for both the polarizations of incident light, with intensities obtained from the transition matrix elements as given by (5.11) [76].
We normalize intensities to the most intense transition, which is the $-2H_1 \longrightarrow -1C_1$ ($\downarrow$) in our scheme (first line from below in the spectrum), and plot only those which are at least 5% of that one [12].
Solid lines represent transitions with a calculated intensity between 1. and 0.4, dashed lines represent those between 0.4 and 0.05. With dotted lines we indicate transitions that are smaller than 5% at some fields but acquire intensity through the admixture with other states with increasing magnetic field. In particular, this is true for transitions between H_3 and C_1 which are forbidden ,at B=0, by the selection rule (5.16) but acquire intensity through the admixture with L states with opposite parity at higher values of the magnetic field.

Many features are born out by the calculation which are not obvious on the basis of the calculated Landau levels only. For instance, the admixture between L and H hole-states in Landau levels with n>0 leads, at fields above 10 Tesla, to a change of slope of the transition lines, making them less steep at higher fields where

---

[12] We adopt the following convention to label transitions : the numbers indicate the Landau level indices of the initial and final level involved in the transition, while the letters refer to the character of the subband at B=0 ; the subscript m is the subband index . The two spin-splitted hole levels, for every Landauindex n ,will be identified (when necessary), by giving the spin character at B ≃ 0 (see the left side of Table 5.15 for the notation). In parenthesis we indicate the spin of the final conduction band level.

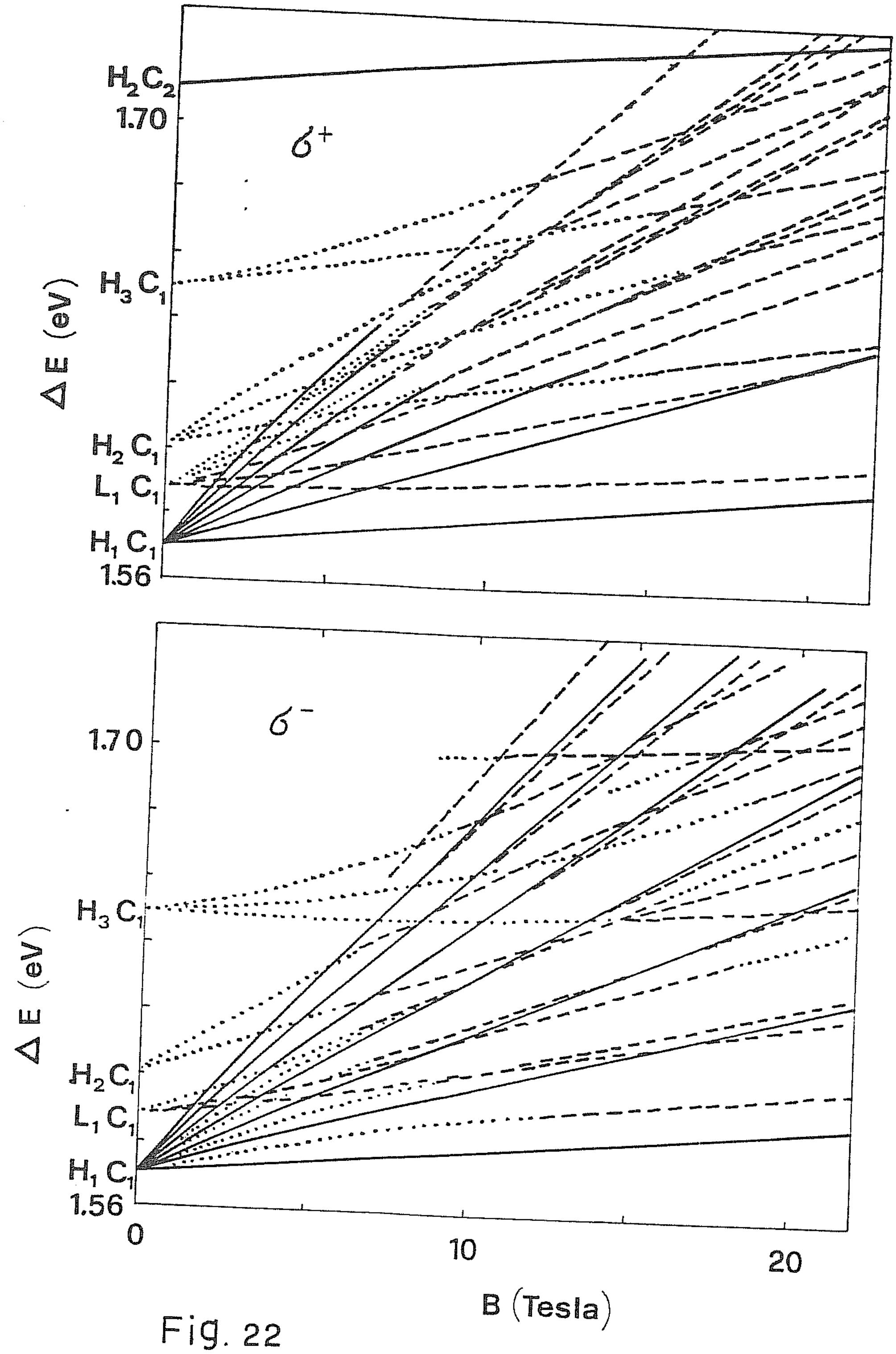

Fig. 22

Calculated transition energies for the two circular polarizations, as a function of the field B. Intensities are normalized to the lowest H_1-C_1 transition and are represented by :

dotted lines : intensity less than .05
dashed lines : between .05 and .4
solid lines : between .4 and 1.

they recover in part the character of Light hole (which ,because of the particular asymmetry in the diagonal elements of the Luttinger-Kohn Hamiltonian (D.1), has a heavier cyclotron mass in the (k_x,k_y) plane).
One important consequence is that the usual practice to derive the zero-field exciton binding energy in QW's as the difference in energy between the ground states and the continuum states obtained by extrapolation at B=0 of high field data, may in some cases give an overestimated value for the binding energy : in fact the experimental values for this quantity, derived in the above manner [58] ,are systematically much higher than the theoretical ones ([77] , [78]).

Note that, in particular for the σ^- spectra, the transitions associated with Landau levels that evolve from the zero-field H -C are always stronger than those involving L-hole states. This makes that the more or less regular, equidistant Landau level-like features can be recognized both in the experiment and the calculation. This statement is less true in the more complicated σ^+spectra.

To give an example of the effect of hole mixing, we report in Fig.23 the calculated intensities relative to the $0H_1 \longrightarrow 1C_1(\downarrow)$ transition -upper curve- and to the $0L_1 \longrightarrow 1C_1(\downarrow)$ transition -lower curve- , as a function of the magnetic field B. On the top of each figure we show, for various values of B, the relative weights of the hole components entering in the envelope-function of the valence Landau levels.
At zero field, the second transition is forbidden, in σ^+ polarization, by the conservation of the total angular momentum (see the table 5.15), but at $B \neq 0$ it acquires intensity through the admixture with the $H\downarrow$ component of the right parity. At $B \gtrsim 15$ Tesla the intensity decreases again due to an increase of the $L\uparrow$ component.
The first transition, which is parity-allowed at B=0, becomes less intense at higher fields due to the mixing with the $L\downarrow$ component (see the related discussion in Section 5.2.1).
For comparison, we report with dashed lines the intensities of the

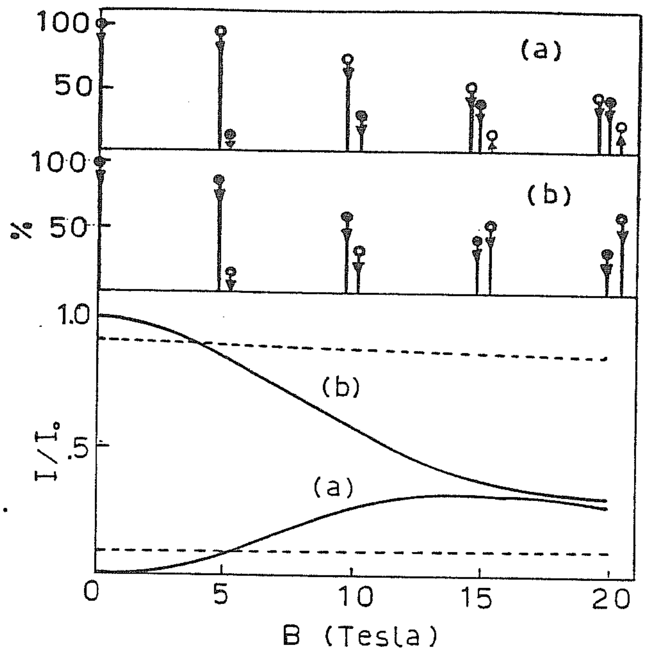

Fig. 23

Normalized intensities of the transition $0H_1 \rightarrow 1C_1$(↓) (curve b) and $0L_1 \rightarrow 1C_1$(↓) (curve a) as a function of the magnetic field B.
In the upper part of the Figure the weight of the various hole components in the envelope functions are shown for different values of B.
For comparison, the intensities of the corresponding transitions in bulk-GaAs are shown with dashed lines.

corresponding transitions in bulk-GaAs : it is evident that mixing effects are peculiar to Quantum Well systems.
A similar analysis is performed on the $3H_2 \longrightarrow 4C_1$ (↑) transition (Fig.24), which is parity forbidden at B=0 : in this case it grows in intensity as the mixing with L↑ component of the opposite parity makes a nonvanishing overlap with the even C↑ state. At fields higher than 8 Tesla, an odd H↑ component is picked up, making the

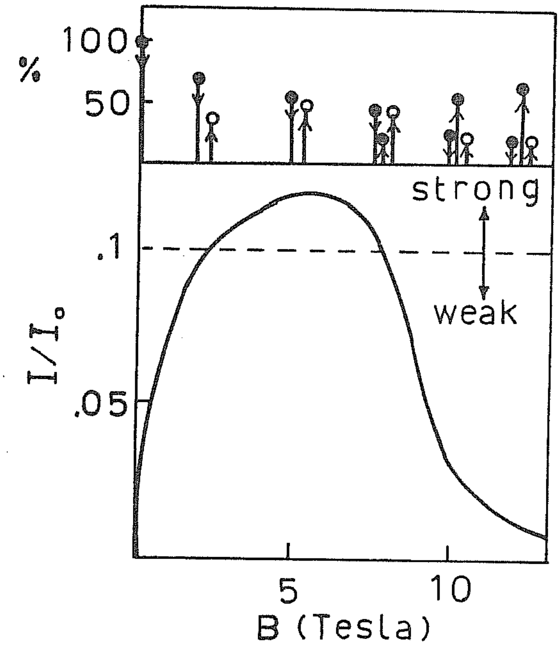

Fig. 24

Same as in Fig.23
The transition is the $3H_2 \longrightarrow 4C_1$(↑)

intensity vanish again. The horizontal line drawn at $I/I_o = .1$ separates the region of "strong" transitions from that of the "weak" ones for the particular experimental spectra examined.

We compare the outcome of our calculation with the experimental data by using band structure parameters that correctly reproduce the bulk data (see next page) and proceed as follows.
We identify the transitions in Fig.22 with the corresponding ones in the experimental results : this comparison shows that we could assign every experimental transition to a calculated one, but that consistently all theoretical ones were too steep, clearly indicating a too small electron mass.
We found that an increase of the electron effective mass by $\simeq 11\%$ is necessary to give the correct slopes of the transition lines. We will come back to this point in the end of this Paragraph.

In order to take into account the excitonic effects in our calculation (we discuss in Paragraph 4.3 the importance of such effects in magneto-absorption experiments) we implemented the simple scheme described in Paragraph 4.3, also used in Ref. [65] ,which follows the treatment of simple-bands excitons in highly anisotropic systems in an external magnetic field [57].

In the limit of high magnetic fields, the exciton binding energy is given by the second term in the expression (4.15) :

$$E_B = 3 R_y^* \, D_1 \{\hbar e B / 2(2n+1) \mu R_y^*\}^{1/2} \qquad (5.17)$$

where μ is the exciton reduced mass, R_y^* is an effective Rydberg and D_1 is a parameter related to the dimensionality of the exciton .
We subtracted the binding energy (5.17) from the Landau level transition energies : we found that the best overall agreement with experimental data at high magnetic field is obtained with $D_1 \cong 0.54$ (We recall that for a strictly 2D exciton $D_1 = 1$, while in the 3D case $D_1 = 1/4$) [13].

The results of our calculation are reported in Fig.25, (excitonic corrections included), together with the observed spectra in the 78 Å sample .
Although the transitions have the right slope, few of them have absolute energy slightly different from the observed ones (typically deviations of 2 ÷ 5 meV are encountered). However, the strongest lines, originating from H hole levels come out at the right energy and with the right slope.
We note by comparing the two figures, that the effect of the exciton character of the transitions is essential in obtaining not only the right energy, but also the right slope for the transitions corresponding to the lowest three exciton states. An additional downward shift of ≃ 9 meV has been imposed on the lowest H_1C_1 and L_1C_1 lines to fit approximately the lowest state HH exciton. The strong horizontal line at energy approximatively 1.7 eV is attributed to the lowest H_2-C_2 exciton transition .

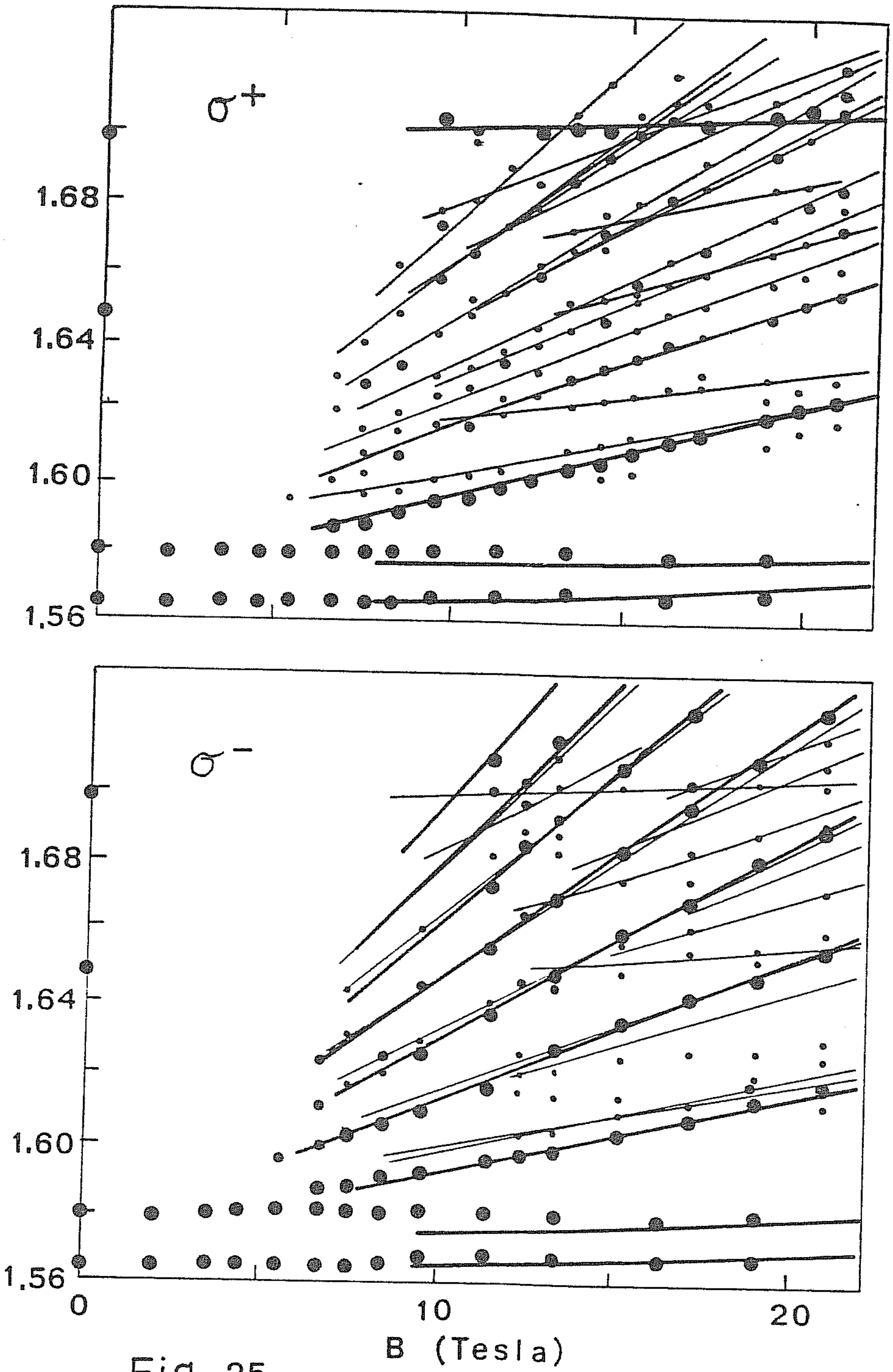

Fig. 25

Comparison between the calculated (lines) and the experimental transition energies (dots) : excitonic corrections are included, as explained in the text. Large dots correspond to strong transitions, small dots to the weak ones.

We see that almost all the weak features of the observed spectra are accounted for by our calculation.

We compare in Fig.26 the predicted intensities at B=19 Tesla with the experimental ones, for both polarizations : in order to mimic the broadening of the observed peaks, we have dressed each of the indicated intensity bars with a Lorentzian-shaped profile 7 meV wide.

The differences between the observed σ^+ and σ^- spectra come out naturally from the calculation, making the overall agreement satisfactory.

It should be remarked that a small change in the relative energy position of transitions originating from different subbands, such as L_1C_1 or H_2C_1, has a sensible effect on the observed spectra. Since the position of the subbands is extremely sensitive to the values of the material parameters (thickness, Al content, band-offset mainly) an exact knowledge of the latters is required in order to make a successful comparison between theory and experiments.

A surprising and puzzling fact is that we need to use a value for the electron mass at the edge of the conduction band higher (m^*

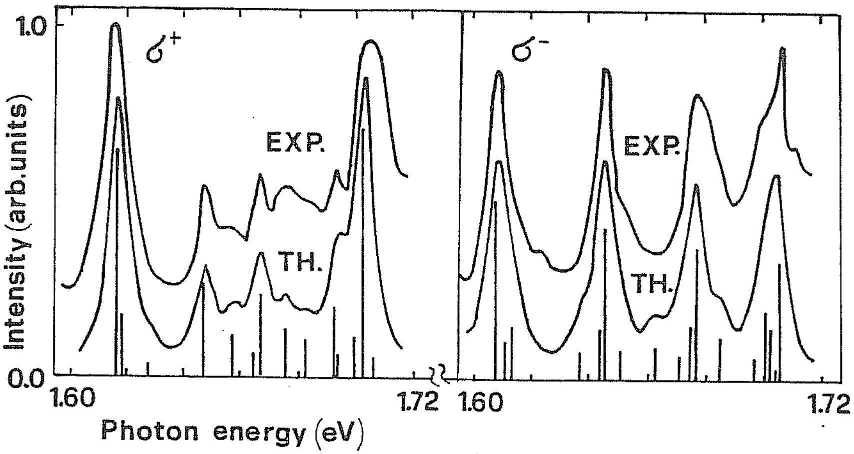

Fig. 26

Comparison between the excitation spectra measured at B=19 Tesla and the predicted intensities. (In order to obtain the theoretical curves, each of the indicated intensity bars has been dressed with a Lorenzian-shaped profile 7 meV wide).

= 0.074m) than the commonly adopted bulk value $m^*=0.0655\,m$ [68] : we have also tried to analyze samples used in different experiments ([79] , [65]), and consistently arrived at the same conclusion, i.e. a higher electron mass is needed to fit the experimental data. This effect is definitively due to the Quantum well : we have verified that the bulk-GaAs magneto-absorption spectra [60] are reproduced in detail by a calculation of inter-Landau level transitions when the "correct" electron mass $m^* = 0.0665\,m$ is used. (the complete set of material parameter used is that listed in APPENDIX F).

The results of this comparison are shown in Fig.27 : solid lines are the calculated interband transition energies, in both σ^+ and σ^- polarization; experimental points are taken from Ref. [60].The calculated lines are just rigidly shifted to fit each series of experimental points : no attempt to include exciton corrections has been made.

In passing, we show in Fig.28 the bulk energy level scheme at B=5 T : the H and L labels refer to the dominant character of each Landau series, when $n \longrightarrow \infty$. [80].Energies are measured from the conduction and valence band edges respectively.

At this stage it is not clear whether this higher electron mass is a consequence of a stronger non-parabolicity of bulk-GaAs that is enhanced by quantum confinement (compare with the discussion in Paragraph 5.1) or it is related to an intrinsic inadequacy of the Effective Mass theory to describe precisely the electron dynamic in systems with only few lattice planes.

Fig. 27

Calculated interband transition energies vs. magnetic field for bulk-GaAs, for both circular polarizations. The experimental points are taken from Ref.
Solid lines are the calculated transition energies (see text).

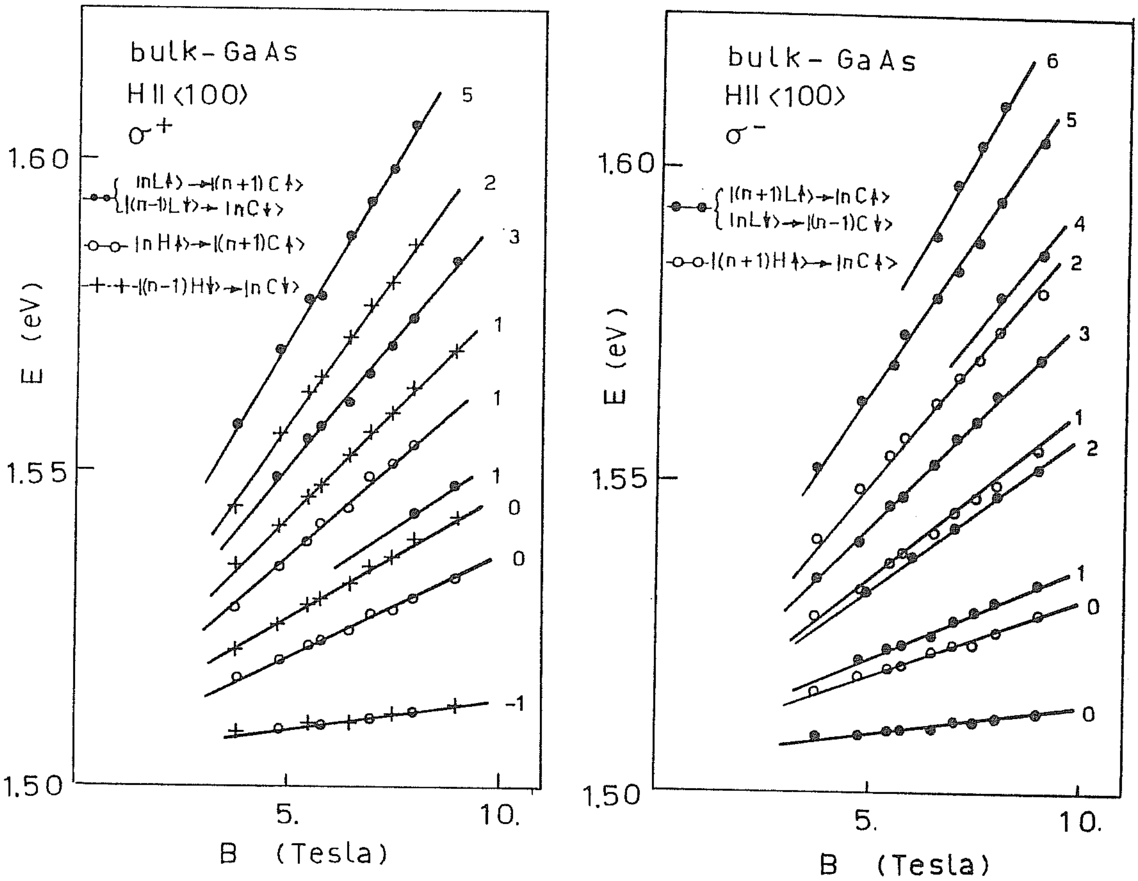

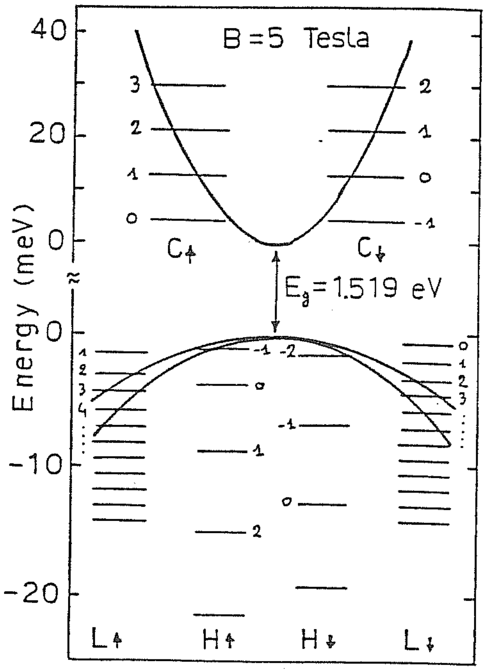

Fig. 28

Energy level scheme for the Landau levels in the valence and conduction bands in bulk GaAs at B=5 Tesla (axial model).
The valence band labels refer to the dominant character of the levels in the limit n→∞

CHAPTER VI

CYCLOTRON RESONANCE IN TWO-DIMENSIONAL HOLE GAS

6.1. Cyclotron resonance in 2D - Hole gas in Quantum Well Structures

In this Chapter we will give a brief account of Cyclotron Resonance (CR) experiments in the Two-Dimensional Hole gas in Quantum well structures : the observed spectra are considerably richer than expected from simple Landau theory (see below). We want to show how the essential features of these spectra can be accounted for, at least in a qualitative way, by the very unusual dependence on the magnetic field of the hole Landau levels in Quantum well systems ([81],[83],[84],[85]).

Consider the simple, illustrative example of a quasi-free electron in a crystal placed in an external magnetic field B in the z-direction. Assuming a parabolic dispersion relation with an effective mass m^* , the energy levels are given by :

$$E_n = (n+1/2)\hbar eB/m^*c + \hbar^2 k_z^2/2m^* \qquad (6.1)$$

where k_z is the electron wave vector in the z-direction and n is an integer.

CR follow from transitions between the Landau levels (6.1) : the resonance condition of the system when interacting with electromagnetic radiation of frequency ω is just :

$$\omega = \omega_c \equiv eB/m^*c \qquad (6.2)$$

This simple picture of quasi-free electrons is applicable to real systems as long as the carrier density is so low that they occupy the states near the band extremum.

The situation in QW's is noticeably different. We have shown in Chapter 5 how the interaction between L and H hole bands gives rise to Landau levels that are not equally spaced and have a very non-linear magnetic field dependence (see, for example, Fig.15).

The unequal level spacing gives rise to a multiplet of cyclotron frequencies at a particular value of the magnetic field instead of the single frequency (6.2) predicted by a parabolic band model. This is actually confirmed by CR experiments : in Fig.29.b we reproduce, from Ref.[81], the CR spectrum at 9 T in the 2D-hole gas formed in the GaAs/AlGaAs Multiple QW structure depicted in Fig.29.a : holes are transferred from the acceptors in the p-doped AlGaAs into the GaAs Quantum Well, where they occupy, for sufficiently low densities, the first quantized level at B=0.

For a finite value of the magnetic field , transitions from occupied Landau levels to empty ones give rise to Cyclotron Resonance spectra.

The two observed peaks correspond to effective masses $m^*=0.41$ and $m^*=0.23$, according to the definition :

$$m^* = e\hbar B/c\Delta E \qquad (6.3)$$

Here ΔE is the energy difference between the two Landau levels.

The matrix elements for an optical transition between an initial hole state characterized by a Landau index n to a final state n' is given by a term analogous to the second term in (5.10), that we

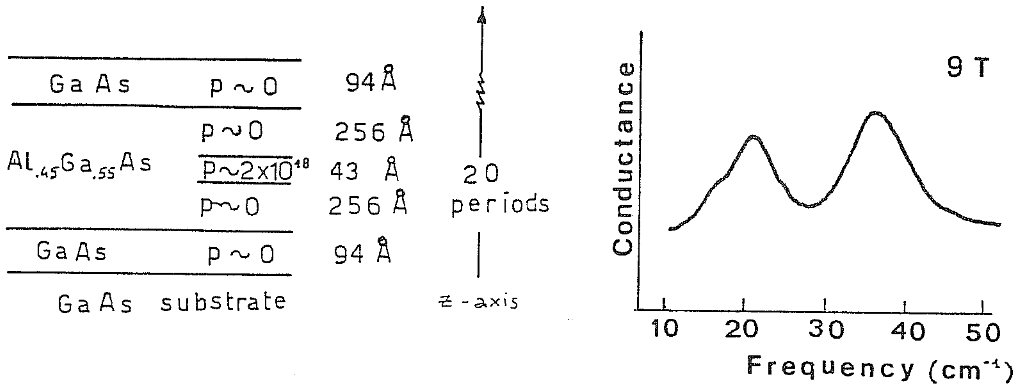

(a) Fig. 29 (b)

(a) The doping and layering of the Multi-Quantum Well sample (from Ref. 81).

(b) Conductance vs. frequency spectrum at B=9 Tesla.

rewrite in the following form [14] :

$$M_{nn'} \propto \langle F_n^{in} | \vec{p}\cdot\vec{\varepsilon} | F_{n'}^{fin} \rangle \simeq m_o \langle F_n^{in} | \vec{v}\cdot\vec{\varepsilon} | F_{n'}^{fin} \rangle \qquad (6.4)$$

where instead of the first-principle scalar interaction $\vec{\varepsilon}\cdot\vec{p}$ we used, following Ref.[90], the matrix interaction term $m_o\vec{\varepsilon}\cdot\vec{v}$. The velocity operator $\hat{\vec{v}}$ is defined in terms of the Effective hole Hamiltonian H [15] :

$$(\hat{v}_i)_{jj'} \equiv (1/\hbar)\, \partial H_{jj'} / \partial k_i \qquad (6.5)$$

and is also a 4x4 matrix which operates on the Envelope-Functions $|F_n\rangle$

For circularly polarized light $\varepsilon_z=0$;then $\vec{\varepsilon}\cdot\vec{v} = \varepsilon_+ v_- + \varepsilon_- v_+$,where

$$\varepsilon_\pm = 1/\sqrt{2}\ (\varepsilon_x \pm i\varepsilon_y) \qquad \text{and}$$

$$v_\pm = 1/\sqrt{2}(v_x \pm i v_y) = 1/\sqrt{2}(\partial H/\partial k_x \pm i\partial H/\partial k_y) =$$

$$= (c/eB)^{1/2} \partial H/\partial a^\pm = \mp (c/eB)^{1/2} [a^\pm , H]$$

(we used the definitions (2.24) of the raising and lowering operators a ,a^+).

Since by definition $H\,|F_n\rangle = \sum_j H_{ij} F_j^n = E\, F_i^n$ is straightforward to show that :

$$M_{nn'} \propto (c/eB)^{1/2} (E_{fin} - E_{in})\, \varepsilon_\pm \langle F_n^{in} | a^\pm | F_{n'}^{fin} \rangle \qquad (6.6)$$

From the definition of the "scalar product" $\langle F_n | F_{n'} \rangle$ (see Footnote [14]) and from the orthogonality of the oscillator states with different index n, one derives immediately the following selection rule :

$$\Delta n = \pm 1 \qquad (6.7)$$

where the + (-) sign holds for left (right) circularly polarized light. We underline the fact that the above selection rule pertains to the axial model only (otherwise the state $|F_n\rangle$ would not be a

---

[14] Here $|F_n\rangle$ is the vector state (5.9) appropriate to the axial model and the symbol $\langle F_n | F_{n'} \rangle$ stands for : $\sum_i \iint F_i^*(\vec{R},z) F_i(\vec{R},z)\, d\vec{R}\, dz$, $\vec{R}$ being the in-plane coordinate vector.

[15] The valence bands are described by the 4x4 LK Hamiltonian derived from expression (E.1) by removing rows and columns 1 and 4 (corresponding to the conduction band states) and by renormalizing the Luttinger parameters γ_1, γ_2, γ_3 and κ as described in APPENDIX F.

solution of the Effective Mass equation).
If one uses the exact Hamiltonian [91] :

$$H = H_{axial} + H_{cub} + H_{K} + H_{G} \qquad (6.8)$$

(where H_{cub} has the form (2.26) and H_{K} ,H_{G} account for linear k terms and G-terms [33] that come in when the crystal lacks inversion symmetry) the selection rule (6.7) must be relaxed and one has instead:

$$\Delta n = \pm m \quad , \text{ where m is an } \underline{\text{odd}} \text{ integer} \qquad (6.9)$$

The terms with m=1 are expected to be strong, while the ones with m>3 come in with H_{cub} and would be absent in the axial approximation.

We have performed a calculation of the hole Landau levels, with the methods described in the previous Chapters, for the case of a 98 Å GaAs-QW between thick AlGaAs barriers, in the axial approximation and assuming that the band gap difference between GaAs and AlAsGa is shared between conduction and valence band, respectively, according to the 60/40 % rule.

Another difference with the case of interband transitions treated previously is that now we must add to the diagonal terms of the hole Hamiltonian matrix the electrostatic potential V(z) arising from the mobile holes in the GaAs Well and from the ionized acceptors in the p-doped AlGaAs layer (see Fig.29.a) .

In principle V(z) should be calculated self-consistently for every value of the field B (see Ref.[83]) : usually this is done in the Hartree approximation, where exchange and correlation effects are neglected (this is a good approximation as long as r_s<<1 : we will see that this is not the case here). However, such a calculation implies a heavy computational effort.

We made here the simpler, "zeroth-order" approximation that consists in solving the Poisson equation in the presence of a uniform hole density in the heterostructure and assuming that the doped layers are completely depleted.

This results in the parabolic profile superimposed on the SL square wave potential represented in Fig.30 ; the explicit expression of

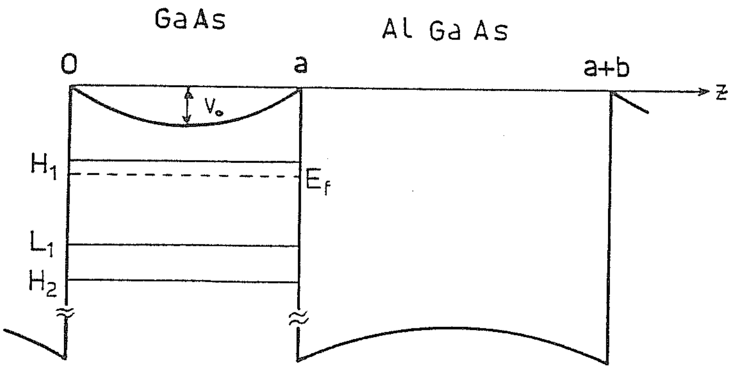

Fig. 30

Valence band energy profile for a Quantum Well of width a=94Å between AlGaAs barriers in the presence of a uniform density of mobile holes in the GaAs layer. The position of the first few levels is shown, together with the 2D Fermi Energy position.

V(z), measured from the top of the valence band, is :

$$V(z) = (2\pi e^2 N_s/\varepsilon) z (1-z/a) \qquad (6.10)$$

a being the Quantum Well width and ε the dielectric constant of GaAs. At the center of the well, $|V| \cong 8$ meV.
The first hole bound states at B=0 are shown in the figure. The dashed line indicates the position of the 2D Fermi Energy : we used here the simple expression valid for parabolic bands $E_F = \hbar^2 N_s/m^*$. Since at sufficiently low carrier densities we expect the highest (Heavy hole) subband only to be populated, we use for m^* the value of the effective HH mass in the z-direction (3.1) $m_H^* = 0.377$ m .Then $E_F \cong 2.9$ meV (measured with respect to the first quantized level) : we see from the figure that only the highest subband is indeed occupied.

To deduce the CR absorption spectrum from the calculated hole Landau levels one must consider, in addition to the selection rules, also the occupation of initial and final states : transitions that are allowed by the selection rule stated above take place only from a (partially) filled Landau level to a (partially) empty one [83].

The filling factor for a 2D system of N_S free-carriers per unit area in the presence of a magnetic field B is given by :

$$\nu = hcN_S/eB \qquad (6.11)$$

where N_S is the two-dimensional density of holes [16]
Using for N_S the value already quoted, one finds $\nu = 19/B$,if B is expressed in Tesla .For example, the first Landau level is filled at B=19 T ; the second is partially filled between 19 and 9.5 T, etc.

In Fig.31 we show the calculated Landau level structure :the thick line indicates the position of the Fermi level at high fields, as obtained with the simple filling scheme described above. Two possible transitions (1⟶2 and -2⟶-1) are also shown.

The resulting transition energies are reported in Fig.32, together with the experimental results taken from Ref.[81] [17] : full circles indicate strong peaks while open circles indicate weak features in the observed spectrum.

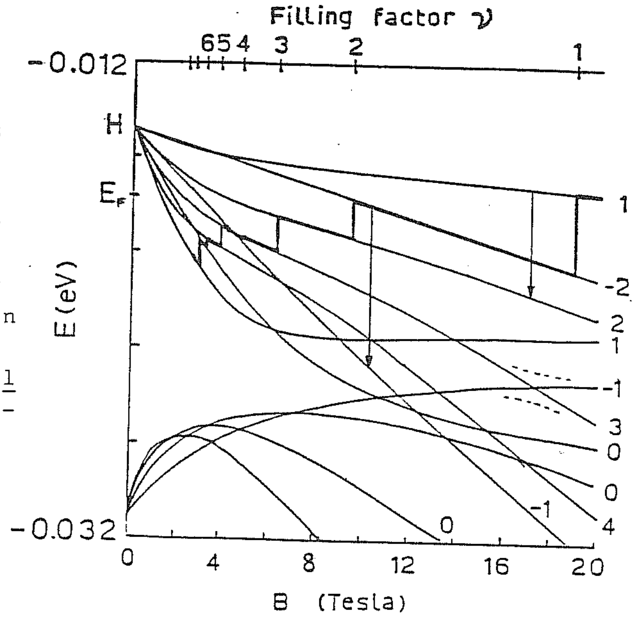

Fig. 31

Landau levels in a 94 Å GaAs Quantum Well between thick AlGaAs barriers.
The Fermi level position for $N_S = 4.6 \times 10^{11}$ holes/cm^2 is indicated for higher fields by the thick line : its position at B=0 is also indicated.
The dashed lines show the calculated splitting of the Landau levels with n=-1 and n=3 due to the anisotropic term in the hole Hamiltonian (see APPENDIX H).

---

[16] We used for simplicity the Landau level degeneracy ζ =eB/hc appropriate to a parabolic band structure.

[17] In Ref.[81] these data are fitted using a simple model that simulate the hole confinement by introducing two adjustable parameters : only a rough semiquantitative agreement with experimental points is achieved.

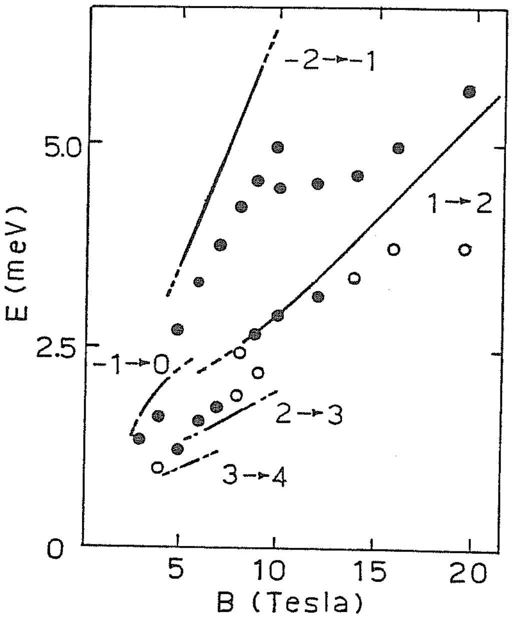

Fig. 32

Measured cyclotron frequencies (dots) compared with theory (lines). Solid circles are strong transitions, open circles are weak ones.
Theoretical transitions account for occupation effects, as described in the text.
The Landau levels involved are also indicated.

The dashed part of the calculated lines means that the corresponding transition takes place to an almost full level or from an almost empty one : these transitions are expected to be weak.
One can see that the effective masses that come out from the calculation depend on the magnetic field both because the energy difference ΔE between two given Landau levels varies with B in a non-linear way, and because transitions between different pairs of Landau levels become possible, depending on the particular value of the Fermi level E_F.

We see from Fig.32 that a rough semiquantitative agreement with experimental points is obtained in our model. More sophisticated calculations of the energy levels of a 2D-Hole gas in a magnetic field don't do much better ([51],[83],[84]). A clear interpretation scheme of CR spectra in 2D-hole gas is still lacking.
In particular, a large splitting of the experimental cyclotron line (corresponding to the 1⟶2 transition in our scheme), occurs in the extreme quantum regime where only the highest hole Landau level is occupied ($\nu < 1$).
This effect has been observed in other CR experiments performed in heterostructures [86] and remains essentially unexplained.

APPENDIX A

The Effective Mass Equation.

This Appendix contains a simple derivation of an Effective Mass (EM) equation as it is used, for example, in the theory of shallow impurity states in semiconductors.

The starting point will be eqn.(2.1), that we rewrite here for clarity :

$$[\, p^2/2m + V_c(\vec{r}) + U(\vec{r}) - E \,]\, \Psi(\vec{r}) = 0 \qquad (A.1)$$

V_c is the periodic potential of the perfect crystal, m is the free electron mass. We assume that the additional potential $U(\vec{r})$ is slowly varying and weak (in the sense precisely stated below), thus acting as a small perturbation. In such a case, the unperturbed states are the eigenfunctions of the equation :

$$H_0\Psi = [\, p^2/2m + V_c(\vec{r}) \,]\, \Psi_{n\vec{k}}(\vec{r}) = E_n(\vec{k})\, \Psi_{n\vec{k}}(\vec{r}) \qquad (A.2)$$

that is, Bloch waves extending over the entire lattice :

$$\Psi_{n\vec{k}}(\vec{r}) = u_{n\vec{k}}(\vec{r})\exp(i\vec{k}\cdot\vec{r}), \qquad u_{n\vec{k}}(\vec{r}+\vec{R}) = u_{n\vec{k}}(\vec{r}) \qquad (A.2b)$$

Here the functions $u_{n\vec{k}}(\vec{r})$ have the periodicity of $V_c(\vec{r})$, $\vec{k}$ lies in the first Brillouin zone and n is a band index running over a complete set of bands.

For $U \neq 0$ we expand the solution of (A.1) in the form :

$$\Psi(\vec{r}) = \sum_{\vec{k}} \varphi_n(\vec{k})\, \Psi_{n\vec{k}}(\vec{r}) \qquad (A.3)$$

This gives a set of coupled linear equations in $\varphi_n(\vec{k})$:

$$[\, E_n(\vec{k}) - E \,]\, \varphi_n(\vec{k}) + \sum_{n'\vec{k}'} \langle \Psi_{n\vec{k}} | U | \Psi_{n'\vec{k}'} \rangle\, \varphi_{n'}(\vec{k}') = 0 \qquad (A.4)$$

The potential matrix elements are :

$$\langle \Psi_{n\vec{k}} | U | \Psi_{n'\vec{k}'} \rangle \equiv \int \Psi^*_{n\vec{k}}(\vec{r})\, U(\vec{r})\, \Psi_{n'\vec{k}'}(\vec{r})\, d\vec{r} =$$

$$= \int \exp[-i(\vec{k}-\vec{k}')\cdot\vec{r}]\; U(\vec{r})\; u^*_{n\vec{k}}(\vec{r})\, u_{n'\vec{k}'}(\vec{r})\, d\vec{r} \qquad (A.5)$$

We shall consider, in the text, states with energy close to the band extremum $\vec{k}=0$: in III-V semiconductor compounds, both the top of the valence band and the bottom of the conduction band are located at this point. We can then make the approximation :

$$u_{n\vec{k}}(\vec{r}) \simeq u_{no}(\vec{r}) \qquad (A.6)$$

Now $u^*_{no}(\vec{r})u_{n'o}(\vec{r}) = \sum_{\vec{G}} A_{nn'}(\vec{G})\exp(i\vec{G}\cdot\vec{r})$ because of the periodicity in the direct lattice. Thus :

$$\langle \Psi_{n\vec{k}} | U | \Psi_{n'\vec{k}'} \rangle = \sum_{\vec{G}} A_{nn'}(\vec{G}) \int \exp[-i(\vec{k}-\vec{k}'-\vec{G})\cdot\vec{r}]\ U(\vec{r})d\vec{r} \qquad (A.7)$$

$$= \sum_{\vec{G}} \tilde{U}(\vec{k}-\vec{k}'-\vec{G})A_{nn'}(\vec{G}) \qquad (A.8)$$

Here $\tilde{U}(\vec{k})$ is by definition the Fourier transform of the potential $U(\vec{r})$.

At this point we make use of the assumption that $U(\vec{r})$ is slowly varying on the length scale of the unit cell: this means that its Fourier transform is appreciably different from zero only when the argument is much smaller compared with a reciprocal lattice vector. Since we assumed that $\vec{k},\vec{k}'$ are very near the zone center, we can then ignore in the expansion (A.8) all the terms with $\vec{G}\neq 0$:

$$\langle \Psi_{n\vec{k}} | U(\vec{r}) | \Psi_{n'\vec{k}'} \rangle \simeq \tilde{U}(\vec{k}-\vec{k}')A_{nn'}(0) \qquad (A.9)$$

Furthermore, the orthogonality condition between Bloch functions requires:

$$1/\Omega \int_{cell} u^*_{no}(\vec{r})u_{n'o}(\vec{r})d\vec{r} = A_{nn'}(0) = \delta_{nn'} \qquad (A.10)$$

the integration been performed over the lattice primitive cell (recall that, for any non-vanishing reciprocal lattice vector $\vec{G}$:

$$\int_{cell} \exp(-i\vec{G}\cdot\vec{r}) = 0 \qquad (A.11)$$

Eqn.(A.4) finally reduces to :

$$[\ E_n(\vec{k}) - E\ ]\ \varphi_n(\vec{k}) + \sum_{\vec{k}'} \tilde{U}(\vec{k}-\vec{k}')\ \varphi_n(\vec{k}') = 0 \qquad (A.12)$$

In the small region around the extremum $\vec{k}=0$, $E_n(\vec{k})$ can be expanded in powers of $\vec{k}$:

$$E_n(\vec{k}) \cong E_n(0) + 1/2\sum_{\alpha,\beta}(\partial^2 E_n(\vec{k})/\partial k_\alpha \partial k_\beta)k_\alpha k_\beta \qquad (A.13)$$

In the case of a simple, isotropic, non-degenerate band extremum (e.g. the conduction band minimum of GaAs direct semiconductor) eqn.(A.13) reduces to :

$$E_n(\vec{k}) = E_n(0) + \hbar^2 k^2/2m^* \qquad (A.14)$$

m^* being the effective mass at the bottom of the band and $E_n(0)$ the band edge.

Eqn.(A.12) can be finally written in real space by using the Fourier transform (FT):

$$F(\vec{r}) = \sum_{\vec{k}} \varphi_n(\vec{k})\exp(i\vec{k}\cdot\vec{r}) \qquad (A.15)$$

(Note that the summation $\sum_{\vec{k}}$ has been implicitly extended over all k-space: this makes little difference because of the assumption that $F(\vec{k})$ is strongly peaked) , and recalling that, in general :

$$E(\vec{k})\varphi(\vec{k}) \text{ --- FT} \rightarrow E(-i\vec{\nabla})\varphi(\vec{r}) \qquad (A.16)$$

One finally finds the following Schrodinger-like equation in $\vec{r}$-space:

$$[-(\hbar^2/2m^*)\nabla^2 + U(\vec{r})]F(\vec{r}) = [E - E_n(0)]F(\vec{r}) \qquad (A.17)$$

Eqn.(A.17) is the Effective Mass Equation familiar from the theory of shallow impurities.

From (A.3),(A.6),(A.15) one obtains the total wavefunction in this approximation :

$$\Psi(\vec{r}) = F(\vec{r})u_{n0}(\vec{r}) \qquad (A.17)$$

The slowly varying function F(r) is usually called "Envelope Eunction" (EF).

APPENDIX B.

The $\vec{k}\cdot\vec{p}$ method.

The $\vec{k}\cdot\vec{p}$ method is a powerful subsidiary tool to be used for the empirical determination of band structure. This method, coupled with the use of symmetry, shows that the band structure in the vicinity of a point in $\vec{k}$-space depends on a small number of parameters (band gaps and effective masses) which may be determined by experiments. Consider the one-particle problem of an electron moving in a periodic potential $V_c(\vec{r})$. The eigenvalue equation is :

$$H\Psi \equiv [\ p^2/2m + V_c(\vec{r})\ ] = E\Psi \quad , \quad V_c(\vec{r}+\vec{R}) = V_c(\vec{r}) \qquad (B.1)$$

$\vec{R}$ being an arbitrary lattice vector. The wave function Ψ may be written in the Bloch form :

$$\Psi \equiv \Psi_{n\vec{k}}(\vec{r}) = u_{n\vec{k}}(\vec{r})\exp(i\vec{k}\cdot\vec{r}) \qquad (B.2)$$

Substituting eqn.(B.2) in eqn.(B.1) one obtains :

$$[\ p^2/2m + (\hbar/m)\vec{k}\cdot\vec{p} + \hbar^2k^2/2m + V_c(\vec{r})\ ]\ u_{n\vec{k}}(\vec{r}) = E_n(\vec{k})u_{n\vec{k}}(\vec{r})$$

(B.3)

Eqn.(B.3) can be written in the form :

$$[\ H_{\vec{k}o} + (\hbar/m)(\vec{k}-\vec{k}_o)\cdot\vec{p} + (\hbar^2/2m)(k^2-k_o^2)]\ u_{n\vec{k}}(\vec{r}) = E_n(\vec{k})u_{n\vec{k}}(\vec{r})$$

(B.4)

where $$H_{\vec{k}o} \equiv p^2/2m + (\hbar^2/2m)\ \vec{k}_o\cdot\vec{p} + \hbar^2 k_o^2/2m + V_c(\vec{r})$$

(B.5)

Then : $H_{\vec{k}o}u_{n\vec{k}_o} = E_n(\vec{k}_o)\ u_{n\vec{k}_o}$ (B.6)

When $\vec{k}$ is near $\vec{k}_o$,the terms added to $H_{\vec{k}o}$ in the left hand side of eqn.(B.4) can be treated by ordinary perturbation theory. This gives, to second order in $(\vec{k}-\vec{k}_o)$ and for a non degenerate band ,:

$$E_n(\vec{k}) = E_n(\vec{k}_o) + (\hbar/m)(\vec{k}-\vec{k}_o)\cdot\vec{p}_{nn} + \hbar^2(k^2-k_o^2)/2m +$$
$$+ (\hbar^2/m^2)\sum_{n'} \frac{|(\vec{k}-\vec{k}_o)\cdot\vec{p}_{nn'}|^2}{E_n(\vec{k}_o)-E_{n'}(\vec{k}_o)} \qquad (B.7)$$

where :

$$\vec{p}_{nn'} \equiv \int_{cell} u^*_{n\vec{k}_o}(\vec{r})\vec{p}u_{n'\vec{k}_o}(\vec{r})d\vec{r} \qquad (B.8)$$

Consider the case in which $\vec{k}_o$ is an extremum : then the term linear in $\vec{k}$ is missing and we can always choose axis so that the quadratic terms in eqn.(B.7) have no cross-product terms. Eqn.(B.7) ,for the particular case $\vec{k}=0$, becomes :

$$E_n(\vec{k}) = E_n(\ ) + (\hbar^2/2)\sum_i k_i^2/m_i^* \tag{B.9}$$

$$1/m_i^* = 1/m + (2/m^2)\sum_{n'} \frac{|\vec{i}\cdot\vec{p}_{nn'}|^2}{E_n(0) - E_{n'}(0)} \tag{B.10}$$

where $\vec{i}$ is a unit vector in the direction of the i-th principal axis. This shows in particular that the interaction with bands of lower (higher) energy tends to reduce (increase) the effective mass. To the same order of approximation, it is possible to express $u_{n\vec{k}}(\vec{r})$ in terms of the $\vec{k}=0$ functions $u_{no}(\vec{r})$:

$$u_{n\vec{k}}(\vec{r}) = u_{no}(\vec{r}) + (1/m)\sum_{n'} \frac{\vec{k}\cdot\vec{p}_{nn'}}{E_n(0) - E_{n'}(0)} u_{n'o}(\vec{r}) \tag{B.11}$$

It is clear that the approximation is good as long as the band considered is non-degenerate and separated by large gaps from all other bands.

From (A.3),(A.15),(B.11) we see that the total electronic wave function in the EF approximation is (see eqn.(2.17)) :

$$\Psi(\vec{r}) = \sum_{\vec{k}} \varphi_n(\vec{k})\, \Psi_{n\vec{k}}(\vec{r}) =$$

$$= \sum_{\vec{k}} \varphi_n(\vec{k}) \exp(i\vec{k}\cdot\vec{r}) \{u_{no}(\vec{r}) + \sum_{n'\neq n} \frac{\vec{k}\cdot\vec{p}_{nn'}}{m\,\{E_n(0) - E_{n'}(0)\}} u_{n'o}(\vec{r})\}$$

$$= F(\vec{r})u_{no}(\vec{r}) + (1/m)\sum_{n'\neq n} \frac{-i[\vec{\nabla}F(\vec{r})]\cdot\vec{p}_{nn'}}{E_n(0) - E_{n'}(0)} u_{n'o}(\vec{r}) \tag{B.12}$$

The correction term proportional to the gradient of the envelope function is essential if one is interested in investigating the derivative of the wave function $\Psi(\vec{r})$; this is the case when the effect of the boundary conditions for the EM equation at the sharp boundary between two different semiconductor must be taken into account.

APPENDIX C

Numerical values of some characteristic quantities.

We give the numerical values of some characteristic quantities. m^*, μ ,when appearing in the third member of each expression,are in unit of the free electron mass m ; is the semiconductor static dielectric constant ($\epsilon_{GaAs} = 12.54$) ; The dimensionality parameters D_1, D_2 in (C.9) and (C.10) are given by [57] :

$$D_2 = \begin{cases} 1 & (\text{ 3D case }) \\ 3/16 & (\text{ 2D case }) \end{cases} \qquad D_1 = \begin{cases} 1/4 & (\text{ 3D case }) \\ 1 & (\text{ 2D case }) \end{cases}$$

Effective Bohr radius :

$$a_0^*[\text{Å}] = \epsilon\hbar^2/e^2m^* = 5.292\times10^{-1}\ \epsilon/m^* \tag{C.1}$$

Dimensionless Wigner-Seitz radius :

$$r_s = (\pi N_s)^{-1/2}/a_0^* = 3.371\times10^2\ N_s^{-1/2}[10^{11}\ \mathrm{cm}^{-2}]\ m^*/\epsilon \tag{C.2}$$

2D Fermi Energy, one subband occupied :

$$E_F[\mathrm{meV}] = \pi\hbar^2N_s/m^* = 2.380\times10^{-1}N_s[10^{11}\ \mathrm{cm}^{-2}]/m^* \tag{C.3}$$

Size of the lowest cyclotron orbit :

$$l\ [\text{Å}] = (\hbar c/eB)^{1/2} = 2.566\times10^2/(B[T])^{1/2} \tag{C.4}$$

Landau level Filling factor :

$$\nu = hcN_s/eB = 4.136\ N_s[10^{11}\ \mathrm{cm}^{-2}]/B[T] \tag{C.5}$$

Effective Rydberg :

$$Ry^*\ [\mathrm{meV}] = \mu e^4/2\hbar^2\epsilon^2 = 1.361\times10^4\ \mu/\epsilon^2 \tag{C.6}$$

Effective cyclotron energy :

$$\hbar\omega_c^*[\mathrm{meV}] = \hbar eB/m^*c = 1.158\times10^{-1}\ B[T]/m^* \tag{C.7}$$

Reduced cyclotron energy :

$$\gamma = \hbar\omega_c^*/2Ry^* = 4.254\times10^{-6}(\epsilon/\mu)^2B[T] \tag{C.8}$$

Exciton binding energy :

$$E_B[\mathrm{meV}] = 3Ry^*\ D_1[\hbar eB/2(2n+1)\mu Ry^*]^{1/2} = 6.690\ D_1(B[T]/2n+1)^{1/2} \tag{C.9}$$

Exciton diamagnetic shift :

$$\Delta E\ [\mathrm{meV}] = D_2\epsilon^2\hbar^4B^2/4\mu^3c^2e^2 = 1.942\times10^{-5}\ D_2B^2[T]/\mu^3 \tag{C.10}$$

APPENDIX D.

Three-band $\vec{k}\cdot\vec{p}$ model Hamiltonian.

The $\vec{k}\cdot\vec{p}$ Hamiltonian describing the interaction of the s-like spin-degenerate conduction band ($s\uparrow$, $s\downarrow$) with the upper spin-orbit J=3/2 partner of the valence band. The four degenerate k=0 valence band edge states are labelled by $J_z = \pm 1/2, \pm 3/2$ (see text). The lower half of the matrix is obtained by hermitean conjugation.

	$s\uparrow$	$3/2$	$-1/2$	$s\downarrow$	$1/2$	$-3/2$
$s\uparrow$	$E_c + k^2/2m^*$	$iP(k_x+ik_y)/\sqrt{2}$	$-iP(k_x-ik_y)/\sqrt{6}$	0	$-i\sqrt{2/3}\,Pk_z$	0
$3/2$		$E_v-(\frac{\gamma_1}{2}-\gamma_2)k_z^2$ $-(\gamma_1+\gamma_2)(k_x^2+k_y^2)/2$	$\sqrt{3}\,\gamma_2(k_x^2-k_y^2)/2$ $-i\sqrt{3}\,\gamma_3 k_x k_y$	0	$\sqrt{3}\,\gamma_3(k_x-ik_y)k_z$	0
$-1/2$			$E_v-(\gamma_1/2+\gamma_2)k_z^2$ $-(\gamma_1-\gamma_2)(k_x^2+k_y^2)/2$	$i\sqrt{2/3}\,Pk_z$	0	$-\sqrt{3}\,\gamma_3(k_x-ik_y)k_z$
$s\downarrow$				$E_c+k^2/2m^*$	$iP(k_x+ik_y)/\sqrt{6}$	$-iP(k_x-ik_y)/\sqrt{2}$
$1/2$					$E_v-(\gamma_1/2+\gamma_2)k_z^2$ $-(\gamma_1-\gamma_2)(k_x^2+k_y^2)/2$	$\sqrt{3}\,\gamma_2(k_x^2-k_y^2)/2$ $-i\sqrt{3}\,\gamma_3 k_x k_y$
$-3/2$						$E_v-(\gamma_1/2-\gamma_2)k_z^2$ $-(\gamma_1+\gamma_2)(k_x^2+k_y^2)/2$

APPENDIX E.

The $\vec{k}\cdot\vec{p}$ Hamiltonian when a magnetic field is applied.

Explicit form of the 6X6 model Hamiltonian (D.1) when a magnetic field along <100> is applied. The lower half of the matrix is obtained by hermitean conjugation.

$$
\begin{array}{ccccccc}
 & s\uparrow & 3/2 & -1/2 & s\downarrow & 1/2 & -3/2 \\
s\uparrow & H_{11} & iP\sqrt{eBn/c} & -iP\sqrt{eB(n+1)/3c} & 0 & -i\sqrt{2/3}\;Pk & 0 \\
3/2 & & H_{22} & (eB/c)\bar{\gamma}\sqrt{3n(n+1)} & 0 & \gamma_3 k_z\sqrt{6eBn/c} & 0 \\
-1/2 & & & H_{33} & i\sqrt{2/3}\;Pk & 0 & -\gamma_3 k_z\sqrt{6eB(n+2)/c} \\
s\downarrow & & & & H_{44} & iP\sqrt{eB(n+1)/3c} & -iP\sqrt{eB(n+2)/c} \\
1/2 & & & & & H_{55} & \bar{\gamma}(eB/c)\sqrt{3(n+1)(n+2)} \\
-3/2 & & & & & & H_{66}
\end{array}
$$

where :

$$\bar{\gamma} = (\gamma_2+\gamma_3)/2$$

$$H_{11} = H_{44} = E_c + eB(n+1)/m^*c + k_z^2/2m^*$$

$$H_{22} = E_v - (\gamma_1/2-\gamma_2)k_z^2 - (eB/c)[(\gamma_1+\gamma_2)(n-1/2) + 3\kappa/2]$$

$$H_{33} = E_v - (\gamma_1/2+\gamma_2)k_z^2 - (eB/c)[(\gamma_1-\gamma_2)(n+3/2) - \kappa/2]$$

$$H_{44} = E_v - (\gamma_1/2+\gamma_2)k_z^2 - (eB/c)[(\gamma_1-\gamma_2)(n+1/2) + \kappa/2]$$

$$H_{55} = E_v - (\gamma_1/2-\gamma_2)k_z^2 - (eB/c)[(\gamma_1+\gamma_2)(n+5/2) - 3\kappa/2]$$

APPENDIX E.

Material parameters for the GaAs/Al$_x$Ga$_{1-x}$As system.

Band parameters of GaAs and AlAs in atomic units. The (a) set of parameters corresponds to the full 6x6 matrix of table I. The (b) set is obtained by removing the explicit coupling of conduction and upper valence band. The direct gap, E_g and the valence band spin-orbit splitting are in eV . m^* is the electron effective mass in the matrix D.1 .

	GaAs		AlAs	
	(a)	(b)	(a)	(b)
P (eV A)	9.27	---	9.27	---
m	0.198		0.312	
γ_1	1.91	6.85	1.05	3.45
γ_2	-0.37	2.1	-0.52	0.68
γ_3	0.43	2.9	0.09	1.29
κ	-1.27	1.2	-1.08	0.12
E	1.519		3.13	
Δ	0.341		0.275	

(Linear interpolation is used for the Al Ga As parameters).

The parameters appearing in the set (b) are related to those in the (a) set by the following relations [46] :

$$\gamma_1^L = \gamma_1 + 2m\ P^2/3\hbar^2 E_g$$

$$\gamma_2^L = \gamma_2 + m\ P^2/3\hbar^2 E_g$$

$$\gamma_3^L = \gamma_3 + m\ P^2/3\hbar^2 E_g$$

$$\kappa^L = \kappa + m\ P^2/3\hbar^2 E_g$$

These are the true Luttinger parameters entering the matrix (3.3) , the contribution of the conduction band being included as a second order cor
The numerical values for GaAs are obtained from cyclotron resonance experiments, as described in Ref.[87] .

With the value quoted for P one obtains ,in a three-band Kane model, the following value for the electron effective mass at the band-edge (see eqn.(5.4)) :

$$m^* = \{ 1 + 2m P^2 [2/E_g + 1/(E_g + \Delta)]/3\hbar^2 \}^{-1} = 0.0665 \; m$$

which is the commonly accepted value for m * [68].
Here m is the free electron mass.

APPENDIX G

Boundary conditions for the many-band case.

It is straightforward to generalize in the many-band case the boundary conditions (2.7,2.10). They become ([39],[19]) :

$$F_j^A(-\varepsilon) = F_j^B(+\varepsilon) \qquad (G.1)$$

$$\sum_{1}^{N}{}_{j'} \{ P_{jj'}^{z} - i \sum_{1}^{3}{}_{\alpha} (D_{jj'}^{z\alpha} + D_{jj'}^{\alpha z}) \nabla_\alpha \} F_{j'} \quad \text{continuous at } z=0 \qquad (G.2)$$

$(j=1,2,\ldots,N)$

(see Paragraph 2.3 for the exact meaning of symbols).
It is important to stress the fact that the second condition, which is the analogous of eqn.(2.7)for the simple band case, is derived by using for the wavefunction the expression (2.19), correct to first order in a $\vec{k}\cdot\vec{p}$ expansion. As we already saw, one must also assume the validity of (2.12) for the N bands of interest.

Let's specialize these boundary conditions for the case of an ideal planar interface between lattice matched semiconductor A and B and assume that the Hamiltonian H has the form (D.1) appropriate to a six-band model. The potential $U(\vec{r})$ in the EM eqn.(2.16) depends only on z and k_x, k_y are thus good quantum numbers. This means that we can write :

$$F_j^{A,B}(\vec{r}) = \exp(ik_x x + ik_y y)\, F_j^{A,B}(z) \qquad (G.3)$$

so that eqn.(G.2) reads :

$$\sum_{1}^{6}{}_{j'} \{ P_{jj'}^{z} + \sum_{\alpha=x,y} (D_{jj'}^{z\alpha} + D_{jj'}^{\alpha z}) k_\alpha - 2i\, D_{jj'}^{zz} \frac{\partial}{\partial z} \} F_{j'} \quad \text{continuos} \qquad (G.4)$$

An additional simplification stems from the fact that the matrix elements $P_{jj'}$ are the same in the two materials (because the u_n's functions are the same) .Eqn.(G.4) thus further simplifies to :

$$\sum_{1}^{6}{}_{j'} \{ \sum_{\alpha=x,y} (D_{jj'}^{z\alpha} + D_{jj'}^{\alpha z}) k_\alpha - 2i\, D_{jj'}^{zz} \frac{\partial}{\partial z} \} F_{j'} \quad \text{continuous} \qquad (G.5)$$

To determine the eigenfunctions and eigenvalues of the system of differential equations (2.18) with the boundary conditions

(G.1,G.5), a standard method of band structure theory has been used [40]

One defines an " interface functional " I embodying the boundary conditions, such that if $\varphi = (F^A , F^B)$ is a solution with energy E of eqn.(2.18) :

$$H\varphi = \begin{pmatrix} H^A & 0 \\ 0 & H^B \end{pmatrix} \begin{pmatrix} F^A \\ F^B \end{pmatrix} = E \begin{pmatrix} F^A \\ F^B \end{pmatrix} \qquad (G.6)$$

and if F^A , F^B satisfy the proper boundary conditions at the A-B interface, then the functional :

$$E[\varphi] = \frac{\langle \varphi | H + I | \varphi \rangle}{\langle \varphi | \varphi \rangle} \qquad (G.7)$$

is stationary with respect to arbitrary variations $\delta\varphi$ of the wavefunction $\varphi = (F^A , F^B)$ (that is the variational principle is valid also for trial wavefunctions that do not satisfy the boundary conditions) and furthermore $E \langle \varphi | \varphi \rangle = \langle \varphi | H+I | \varphi \rangle$.

Once the interface functional is known ,one can take two suitable sets of basis functions in A and B ,with the periodicity of the superlattice, into which to expand F^A, F^B respectively.

The explicit expression of the functional I is [41] :

$$\langle \varphi | I | \varphi \rangle = (i/2) \{ \langle F^A | \bar{J}(0) | F^A \rangle - \langle F^B | \bar{J}(0) | F^B \rangle + + \langle F^B | \bar{J}(0) | F^A \rangle - \langle F^A | \bar{J}(0) | F^B \rangle \} \qquad (G.8)$$

$\bar{J}(0)$ being the current operator averaged over the unit cell (see def. 2.8).

The eigenproblem can thus be solved through a standard matrix diagonalization ,making in addition easier to implement self-consistent calculations when charge transfer across the interface is expected.

APPENDIX H

Effect of the anisotropic part of the Luttinger Hamiltonian when a magnetic field is applied.

We give here a simple estimate of the effect of the anisotropic part H_{cub} in the Luttinger hole Hamiltonian (3.3) that is neglected in the axial approximation.

When a magnetic field of strength B is applied in the z-direction, H_{cub} can be represented as (see (2.26),(2.27),(2.28) in the text) :

$$H_{cub} = \begin{vmatrix} H_a & 0 \\ & \\ 0 & H_b \end{vmatrix} \quad , \text{ where } \quad H_a = H_b = A \begin{vmatrix} 0 & 0 & 0 \\ 0 & 0 & a^{+2} \\ 0 & a^2 & 0 \end{vmatrix} \qquad (H.1,2)$$

and

$$A = \sqrt{3}\, \hbar eB/2cm\ (\gamma_2 - \gamma_3) \qquad (H.3)$$

Let's denote with $|F_n\rangle$ the eigenstate (2.29) of the axial Hamiltonian, n being the Landau index.

By applying the matrix H_{cub} to the state $|F_n\rangle$ and projecting the resulting vector onto $\langle F_{n'}|$, one sees immediately that H_{cub} couples Landau levels with n and n±4 : this implies for example that the levels with n=-1 and 3 in Fig.31 that cross each other at B=17.6 and B=4.8 Tesla , should display anticrossing behavior, having also a mixed n=-1 and n=3 character.

We calculated approximatively the splittings at these two points by using the formula :

$$\Delta E \cong 2|\langle F_n | H_{cub} | F_{n+4}\rangle| \qquad (H.4)$$

It turns out that :

E = 0.7 meV at 17.6 T (shown with dashed lines in Fig.32)
E = 0.03 meV at 4.8 T (H.5)

in agreement with the results of more complete calculations([51],[84])

The effect of H_{cub} is very small and can,in general,be safely neglected. Note that the first splitting is much greater than the other : this is simply because the matrix elements of (H.1) are proportional to B and also because H_{cub} , when acting on a given state $|F_n\rangle$, mixes the H and L hole components with the same spin and thus affects mainly levels with strong admixture of L and H character, like the two that cross at 17.6 T.

BIBLIOGRAPHY

(1) *Molecular Beam Epitaxy and Heterostructures*, NATO Advanced Science Institute Series, Nijhoff, Dordrecht (1985). L.L.Chang,K.Ploog eds.

(2) *Metal Organic Vapor Phase Epitaxy*, North Holland, Amsterdam (1984). J.B.Mullin, S.J.C.Irvine, R.H.Moss, P.N.Robson, D.R.Wight eds.

(3) L.Esaki, and R.Tsu, *IBM J.Res.Develop*. Vol. 14 p. 61 (1970).

(4) K.Ploog, and K.Graf, *Molecular Beam Epitaxy of II-V compounds*, Springer, Berlin (1984).

(5) L.L.Chang, *J.Vac.Sci.Technol.B* Vol. B1 p. 120 (1983).

(6) J.K.Furdyna, and J.Kossut, *Superlattices* & *Microstructures* Vol. 2 p. 89 (1986).

(7) G.Dohler, *Sci.Am.*, p. 144 (November 1984).

(8) H.L.Stormer, K.Baldwin, A.C.Gossard, and W.Wiegmann, *Appl.Phys.Lett*. Vol. 44 p. 1062 (1984).

(9) L.L.Chang, L.Esaki, W.E.Howard, and R.Ludeke, *J.Vac.Sci.Technol*. Vol. 10 p. 11 and 655 (1973).

(10) L.Esaki, *Proc.of the 11-th International Conference on the Physics of Semiconductors*, Warsaw (1972).

(11) L.L.Chang, N.Kawai, G.A.Sai-Halasz, R.Ludeke, and L.Esaki, *Appl.Phys.Lett*. Vol. 35 p. 939 (1979).

(12) L.Esaki, and L.L.Chang, *Phys.Rev.Lett*. Vol. 33 p. 495 (1974).

(13) G.Belle, J.C.Maan, and G.Weimann, *Sol.St.Comm*. Vol. 56 p. 65 (1985).

(14) K.v.Klitzing, G.Dorda, and M.Pepper, *Phys.Rev.Lett.* Vol. 45 p. 494 (1980).

(15) D.C.Tsui, A.C.Gossard, and H.L.Stormer, *Phys.Rev.Lett.* Vol. 48 p. 1559 (1982).

(16) R.B.Laughlin, *Phys.Rev.Lett.* Vol. 50 p. 1395 (1983).

(17) H.L.Stormer, *Festkorperprobleme* Vol. XXIV p. 25 (1984). H.J.Queisser ed.

(18) L.Esaki, *Proceedings of the 17-th International Conference on the Physics of Semiconductors*, S.Francisco, Springer-Verlag (1984). J.D.Chadi ,W.A.Harrison eds.

(19) M.Altarelli, *Phys.Rev.B* Vol. 28 p. 842 (1983).

(20) Y.Gouldner, G.Bastard, J.P.Vieren, M.Voos, J.P.Faurie, and A.Million, *Phys.Rev.Lett.* Vol. 51 p. 907 (1983).

(21) M.Heiblum, E.E.Mendez, and F.Stern, *Appl.Phys.Lett.* Vol. 44 p. 1064 (1984).

(22) K.Ploog, and G.Dohler, *Adv.Phys.* Vol. 32 p. 285 (1983).

(23) G.Osbourn, R.Biefeld, and P.Gourley, *Appl.Phys.Lett.* Vol. 41 p. 172 (1982).

(24) G.Osbourn, *J.Appl.Phys.* Vol. 53 p. 1586 (1982).

(25) P.Voisin, E.Delalande, M.Voos, L.L.Chang, A.Segmuller, C.A.Chang, and L.Esaki, *Phys.Rev.B* Vol. 30 p. 2276 (1984).

(26) R.Dingle, *Festkorperprobleme* Vol. XV p. 21 (1975). H.J.Queisser ed.

(27) R.C.Miller, D.A.Kleinman, and A.C.Gossard, *Phys.Rev.B* Vol. 29 p. 7085 (1984).

(28) J.Menendez, A.Pinczuk, D.J.Werder, A.C.Gossard, and J.H.English, *Phys.Rev.B* Vol. 33 p. 8863 (1986).

(29) D.W.Niles, and G.Margaritondo, *Phys.Rev.B* Vol. 34 p. 2923 (1986).

(30) G.Bastard, *Phys.Rev.B* Vol. 24 p. 5693 (1981).

(31) M.Altarelli, *Band structure, Impurities and Excitons in Superlattices*, Lecture notes for the Winter School on Semiconductor Heterojunctions and Superlattices, Les Houches (1985).

(32) R.A.Morrow, and K.R.Brownstein, *Phys.Rev.B* Vol. 30 p. 678 (1984).

(33) E.O.Kane, *Semiconductors and Semimetals*, Academic Press, New York (1966). K.Willardson, A.C.Beer eds.

(34) L.M.Roth, B.Lax, and S.Zwerdling, *Phys.Rev.* Vol. 114 p. 90 (1959).

(35) L.D.Landau, and E.M.Lifshitz, *Quantum Mechanics*, Pergamon Press (1977).

(36) J.M.Luttinger, *Phys.Rev.* Vol. 102 p. 1030 (1956).

(37) H.J.Lee, Y.Juravel, J.C.Woolley, and A.J.Springthorpe, *Phys.Rev.B* Vol. 21 p. 658 (1980).

(38) J.M.Luttinger, and W.Kohn, *Phys.Rev.* Vol. 97 p. 869 (1955).

(39) A.Fasolino, and M.Altarelli, *Two-Dimensional Systems, Heterostructures and Superlattices*, Springer, Berlin (1984). G.Bauer, F.Kuchar and H.Heinrich eds.

(40) H.Schlosser, and P.M.Marcus, *Phys.Rev.* Vol. 131 p. 2529 (1969). (Appendix 1)

(41) M.Altarelli, *Applications of High Magnetic fields in Semiconductor Physics*, Springer, Berlin (1983). G.Landwehr ed.

(42) J.N.Schulman, and Y.C.Chang, *Phys.Rev.B* Vol. 31 p. 2056 and 2069 (1985).

(43) M.Altarelli, U.Ekenberg, and A.Fasolino, Phys.Rev.B Vol. 32 p. 5138 (1985).

(44) N.Lipari, and M.Altarelli, Phys.Rev. B Vol. 15 p. 4883 (1977).

(45) S.S.Nedorezov, Sov.Phys.Sol.State Vol. 12 p. 1814 (1972).

(46) M.F.N.Schuurmans, and Hooft, G.W. t', Phys.Rev.B Vol. 31 p. 8041 (1985).

(47) M.Cardona, N.E.Christensen, and G.Fasol, Phys.Rev.Lett. Vol. 56 p. 2831 (1986).

(48) T.Ando, J.Phys.Soc.Jpn. Vol. 54 p. 1528 (1985).

(49) F.Capasso, Surf.Sci. Vol. 142 p. 513 (1984).

(50) A.Fasolino, and M.Altarelli, Surf.Sci. Vol. 170 p. 606 (1986).

(51) S.R.Yang, D.Broido, and L.J.Sham, Phys.Rev. B Vol. 32 p. 6630 (1985).

(52) D.C.Reynolds, and T.C.Collins, Excitons : their properties and uses, Academic press (1981).

(53) F.Bassani, and G.Pastori-Parravicini, Electronic states and optical transitions in Solids, Pergamon Press (1975). R.A.Ballinger ed.

(54) L.Pauling, and E.B.Wilson, Introduction to Quantum Mechanics, McGraw Hill, New York (1935).

(55) R.L.Greene, and K.K.Bajaj, Sol.St.Comm. Vol. 45 p. 831 (1983).

(56) G.Bastard, E.E.Mendez, L.L.Chang, and L.Esaki, Phys.Rev.B Vol. 26 p. 1974 (1982).

(57) O.Akimoto, and H.Hasegawa, J.Phys.Soc.Jpn. Vol. 22 p. 181 (1967).

(58) J.C.Maan, A.Fasolino, G.Belle, M.Altarelli, and K.Ploog, Phys.Rev.B Vol. 30 p. 2253 (1984).

(59) S.Tarucha, H.Okamoto, Y.Iwasa, and N.Miura, Sol.St.Comm. Vol. 52 p. 815 (1984).

(60) Q.H.F.Vrehen, J.Phys.Chem.Solids Vol. 29 p. 129 (1968).

(61) D.F.Edwards, and V.J.Lazazzera, Phys.Rev. Vol. 120 p. 420 (1960).

(62) R.J.Elliott, and R.Loudon, J.Phys.Chem.Solids Vol. 8 p. 382 (1959).

(63) R.J.Elliott, and R.Loudon, J.Phys.Chem.Solids Vol. 15 p. 196 (1960).

(64) M.Altarelli, and N.Lipari, Phys.Rev.B Vol. 9 p. 1733 (1974).

(65) D.C.Rogers, J.Singleton, R.J.Nicholas, C.T.Fox, and K.Woodbridge, Pyis.Rev.B Vol. 34 p. 4002 (1986).

(66) R.Lassnig, Phys.Rev.B Vol. 31 p. 8076 (1985).

(67) G.Lindemann, R.Lassnig, W.Seidenbush, and E.Gornik, Phys.Rev.B Vol. 28 p. 4693 (1983).

(68) J.M.Chamberlain, P.E.Simmonds, R.A.Stradling, and C.C.Bradley, Proc. of the 11-th International Conference on the Physics of Semiconductors , Warsaw (1972).

(69) C.Hermann, and C.Weisbuch, Phys.Rev. B Vol. 15 p. 823 (1977).

(70) U.Rossler, Sol.St.Comm. Vol. 49 p. 943 (1984).

(71) C.R.Pidgeon, and R.N.Brown, Phys.Rev. Vol. 146 p. 575 (1966).

(72) P.Voisin, G.Bastard, and M.Voos, Phys.Rev.B Vol. 29 p. 935 (1984).

(73) R.R.Goodman, Phys.Rev Vol. 122 p. 397 (1961).

(74) M.H.Meynadier, C.Delalande, G.Bastard, and M.Voos, Phys.Rev.B Vol. 31 p. 5539 (1985).

(75) J.A.Brum, and G.Bastard, J.Phys.C Vol. 18 p. L789 (1985).

(76) F.Ancilotto, A.Fasolino, and J.C.Maan, to be published in "Superlattices & Microstructures", 1986.

(77) R.C.Miller, D.A.Kleinmann, W.T.Tsang, and A.C.Gossard, Phys.Rev.B Vol. 24 p. 1134 (1981).

(78) R.L.Green, K.K.Bajaj, and D.E.Phelps, Phys.Rev.B Vol. 29 p. 1807 (1984).

(79) B.Deveaud, A.Regreny, A.Romestein, and J.C.Maan, private communication.

(80) R.L.Aggarwal, Semiconductors and Semimetals, Academic Press (1972). R.K.Willardson,A.C.Beer eds.

(81) Z.Schlesinger, S.J.Allen, Y.Yafet, A.C.Gossard, and W.Wiegmann, Phys.Rev.B Vol. 32 p. 5231 (1985).

(82) H.R.Trebin, U.Rossler, and R.Ranvaud, Phys.Rev.B Vol. 20 p. 686 (1979).

(83) U.Ekenberg, and M.Altarelli, Phys.Rev.B Vol. 32 p. 3712 (1985).

(84) E.Bangert, and G.Landwehr, Surf.Sci. Vol. 170 p. 593 (1986).

(85) A.Broido, and L.J.Shamm, Phys.Rev.B Vol. 31 p. 888 (1985).

(86) Z.Schlesinger, and W.I.Wang, Phys.Rev.B Vol. 33 p. 8867 (1986).

(87) K.Hess, D.Bimberg, N.O.Lipari, J.U.Fischbach, and M.Altarelli, Proc.13-th International Conference on the Physics of Semiconductors, F.G.Fumi eds., Rome (1976).

(88) M.Altarelli, and A.Fasolino, Highlights of Condensed- Matter Theory, F.Bassani, F.Fumi, M.P.Tosi eds. (1983).

(89) R.Sooryakumar, D.S.Chemla, A.Pinczuk, A.Gossard, and W.Wiegmann, Proc.17 th Int.Conference on the Physics of Semiconductors, S.Francisco (1984).

(90) K.Suzuki, and J.C.Hensel, Phys.Rev.B Vol. 9 p. 4184 and 4219 (1974).

(91) R.Grisar, H.Wachernig, G.Bauer, J.Wlasak, J.Kowalski, and W.Zawadzky, Phys.Rev.B Vol. 18 p. 4355 (1978).